We would like to thank the reviewer for the comments and questions, which helped us to improve the manuscript. The reviewer's comments (*italic*) are given below together with our responses and changes made in the manuscript (blue).

Answers to the comments of Reviewer #1

PG 3: Oxidation mechanism of myrcene: The SAR of Peeters 2007 has recently been used and updated in the protocol by Jenkin et al., 2018 on the "Estimation of rate coefficients and branching ratios for gas-phase reactions of OH with aliphatic organic compounds for use in automated mechanism construction". Have you looked at this to see if it gives different results to Peeters 2017? Never the less, the Jenkin et al., 2018 work should be citied here also.

Thanks for reminding us of the work by Jenkin et al.. The SAR used in Peeters et al. (2017) and Jenkin et al. (2018) give indeed similar predictions of the reaction rate constant of the reaction of myrcene with OH. We added in Line 415 "The reaction rate constants calculated from structure-activity relationship (SAR) by Peeters et al. (2007) and Jenkin et al. (2018) give similar results between 1.8 to 1.9 $\times 10^{-10}$ cm^3 s^{-1}. Values are approximately 20 % lower than the experimentally derived reaction rate constants. However, differences are within the accuracy of SAR predictions." Reaction rate constants derived from Jenkin et al. (2018) are added in Table 4.

Could epoxide formation in this system (c.f. IEPOX from isoprene + OH) also be an important pathway in the myrcene mechanism, with important implications on SOA formation?

Epoxide products are formed as a third-generation product and are not very reactive with OH. For potential SOA formation not investigated in these experiments, epoxide formation could be of importance. However, for the photochemistry experiments in this work the chemistry was dominated by the first oxidation step of myrcene. This was ensured by the re-injection of myrcene once it had reacted away. Therefore, the formation of third-generation products did not play a role for the gas-phase chemistry. Thus, we cannot draw any conclusions about potential formation of epoxide products from these experiments.

PG 3: Spelling: "epxerimental" and "Peters"

Corrected.

PG 4, line 100: "Products likely undergo fast ring-closure reactions on the dimethyl double bond with rates on the order of 1 s-1 (pers. comm. Vereecken, 2021b)" – why is this chemistry not included in Fig. 4

Answer: The uncertainty, which products are formed, is very high and quantum-chemical calculations would be required to verify, if this estimate was true. The experiments focused on the investigation of the first oxidation step of myrcene. Therefore, the exact products did not matter for the conclusions of this work.

PG 4, line 111: Should "Fig 1" be "Fig 2"?

Corrected.

PG 5, line 129: "e.g." wrong place

Corrected.

PG 5, line 130: add the experiment RH values to Table 1

Added.

PG 5, line 131: define "medium" NO in the context of your experiments

We clarify in Line 131: "two of which were done at medium levels of nitric oxide (NO) ranging from 0.1 to 0.4 ppbv (18 August 2012…"

PG 5, line 140: "Approx 50 ppbv O3 added…" - therefore ozonolysis of myrcene will form products similar to the OH reaction, potentially interfering with the mechanistic results. This needs to be discussed further here, and you need to show evidence that interferences from ozonolysis is minimized in these experiments (which you discuss later).

We added in Line 140: "Products from the ozonolysis of myrcene are similar to the products formed from the reaction with OH. These could lead to systematic errors in the conclusions with respect to the OH oxidation scheme. Given the typical OH concentration in this study (5×10^6 cm^{-3}), the contribution of ozonolysis to the entire oxidation of myrcene is less than 20%. The potential interfering is minimized in the medium NO cases, where ozonolysis only contributes 10% of the myrcene oxidation."

PG 5, line 142 – 145: I am unsure how these concentrations discussed here map onto those given in Table 1, i.e. 2.3 ppbv for the first injection in the "medium" NO expts and 0.8 ppbv for the first injection in the lower NO experiments...?

We corrected the numbers in the text: “Injections were done 2 times (approximately 2 ppbv each) in experiments with medium NO and four injections with smaller concentrations (approximately 1 ppbv) were done in the other experiments.”

PG 5, line 146 – 149: again, cross reference the concentration data with the data given in Table 1

We changed the numbers in Table 1.

PG 6, line 163: How do the different methods of measuring HCHO compare? (and show evidence they are comparable in the experiments here, or that they are comparable from other SAPHIR experiments)

We added in Line 163: “The HCHO concentrations measured by the different methods has been shown to agree within 10% in a series of experiments in the SAPHIR chamber, in which both instruments concurrently measured (Glowania et al. 2020).”

PG 7, line 197: VOC reactivity and RO2 speciation in myrcene experiments – give a brief explanation of how k’(OH) was measured here

We added after the first sentence of this paragraph: “Total OH reactivity was measured by LP-LIF while the speciated OH reactivity for individual species X was calculated from the products of concentrations of X and its reaction rate versus OH.”

PG 11, line 313: you need to provide information on where the ozonolysis OH and RO2 yields are derived from in Table 3. What about the ozonolysis yields of HO2?

We added in Line 313: “The applied rate constants are listed in Table 3. The OH and RO2 yields are taken from Deng et al. (2018)., In their work, the yield of HO2 is zero.”

PG 13, line 378: “reacivity”

Corrected.

PG 13, line 379: Why was the methane experiment, which is key to understanding the uncertainties of this analysis, not repeated with the DOAS OH measurements? (and

ideally a different CH4 measurement?) Could experiments on a simple, well known alkene + OH system (such as ethene or TME) also be useful here?

In other experiments, DOAS and LIF measurements well agreed as demonstrated in a number of publications. One example is shown in the work Novelli et al. (2020), in which isoprene oxidation experiments are analyzed. It is certainly useful and will also be done to repeat the experiment regularly and to use other systems. In this work, we want to demonstrate the concept of the analysis and to estimate the accuracy that can be achieved.

PG 13, line 386: Both JPL and IUPAC need to be referenced appropriately

We added the references.

PG 14, line 399 and 401: appropriately reference "?"
Corrected.

PG 14, line 415: Jenkin et al., 2018 gives an My + OH rate constant (298 K) of 1.88E-10 cm^{-3} s-1 (see earlier comment with respect to update to the Peeters 2007 SAR…)
We added the results from Jenkin et al., 2018 in the text and in Table 4.

PG 15, line 440: Derive the yields from Jenkin et al., 2018 as well. Could you not also use a simple model to show the impact of RO2 isomerisation reactions on the carbonyl yields? Which instrument(s) was used to measure the HCHO yields in the different experiments here? How do the different methods compare?

We derived the yields from Jenkin et al. (2018) and changed the first sentence: "… the isoprenyl part (Peeters et al., 2007). In comparison, the SAR developed by Jenkin et al. (2018) predicts a branching ratio of 63:37 for the OH addition to the −CH=C(CH3)2 moiety and the isoprenyl part, consistent with values reported in Peeters et al. (2007)."

The calculation of the formaldehyde yield from measurements takes into account the sources and sinks, in order to derive the yield from the OH oxidation of myrcene. This is compared to numbers expected from the oxidation scheme. A chemical model essential would give the same answer. This is also the case for other carbonyl products.

The question about the formaldehyde measurements is answered above.

PG 17, line 499: "well agrees"

Corrected.

PG 18, line 534: "Sensitivity model runs" Explain how these models were built and run here. In fact, there was no "model run", but numbers were varied to calculate turnover rates of reactions.

We changed the sentence: "A sensitivity test shows that using a bulk isomerization reaction rate constant of 0.05 s^{-1} instead of 0.02 s^{-1} would be sufficient to balance the RO_2 production rate."

Table 2: "acetaldehyde" (spelling): How and why was this measured here?
We removed the information about acetaldehyde in the table as its photolysis only makes a negligible contribution to the radical production rate.

Table 3: R4 - ?

Corrected.

Table 4: Add the value derived from Jenkin et al., 2018 – 1.88E-10 cm3 s1
We added the value in Table 4.

Figure 8: This figure is a bit messy, and could be clearer. Separate into 2 Figures (i.e. Figure 8a and Figure 8b)

We changed the figure as suggested.

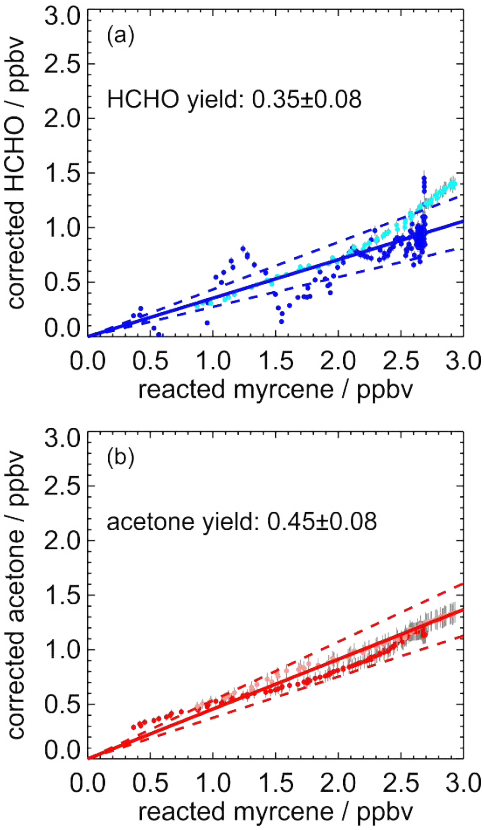

References

Jenkin, M. E., *et al.,* Estimation of rate coefficients and branching ratios for gas-phase reactions of OH with aliphatic organic compounds for use in automated mechanism construction., *Atmos. Chem. Phys*., **18**, 9297–9328, 2018 .https://doi.org/10.5194/acp-18-9297-2018

Novelli, A., Vereecken, L., Bohn, B., Dorn, H. P., Gkatzelis, G. I., Hofzumahaus, A., Holland, F., Reimer, D., Rohrer, F., Rosanka, S., Taraborrelli, D., Tillmann, R.,Wegener, R., Yu, Z., Kiendler-Scharr, A.,Wahner, A., and Fuchs, H.: Importance of isomerization reactions for OH radical regeneration from the photo-oxidation of isoprene investigated in the atmospheric simulation chamber SAPHIR, *Atmos. Chem. Phys.*, 20, 3333–3355, https://doi.org/10.5194/acp-20-3333-2020, 2020.

Answers to the comments of Reviewer #2

We would like to thank the reviewer for his/her comments and suggestions that helped us to improve the manuscript.

Page 6, line 170: While it does appear that a calibration error may be responsible for the discrepancy between the LIF and DOAS measurements of OH on 22 August given that the LIF and DOAS measurements agree during the 2013 measurements, the authors should comment on whether an unknown interference similar to that observed by Fuchs et al. (AMT, 9, 1431–1447, 2016) might be responsible for the discrepancy.

We added discussion in the end of the paragraph: "Interference could occur in OH measurements by the LIF instrument from alkene ozonolysis at exceptionally high concentrations of reactants (Fuchs et al., 2016). However, the ozone and myrcene concentrations used in this study were much lower compared to concentrations used in the characterization experiments in Fuchs et al. (2016). Therefore, it is not expected that similar interferences were significant for measurements in these experiments. Thus, the observed differences in the OH measurements of the LIF and DOAS instruments were most likely caused by calibration errors."

Page 14, lines 399 and 401: The authors should clarify the "?" reference referred to in this section.

Corrected.

Page 16, line 496 and Figure 10: The authors should clarify the adjustments made to the MyO2+HO2 reaction to bring the radical loss into balance with production with the actual factor used to (between 0.4 and 0.7) in the text and in the caption to Fig. 10, perhaps also including the uncorrected loss rates for comparison.

We revised the sentence: "The reaction rate constant of 2.1×10^{-11} cm^3s^{-1} suggested by Jenkin et al. (2019) would need to be reduced between a factor of 0.4 and 0.7 (0.9 to 1.6×10^{-11} cm^3s^{-1} (T = 298 K, Table 3) or the yield of radical products would need to be in the range of 0.3 and 0.6 to match the range of radical production."

Figures 10 was updated to show the impact of the change in the reaction rate constant of the HO_2+MyO_2 reaction on the ROx destruction rate.

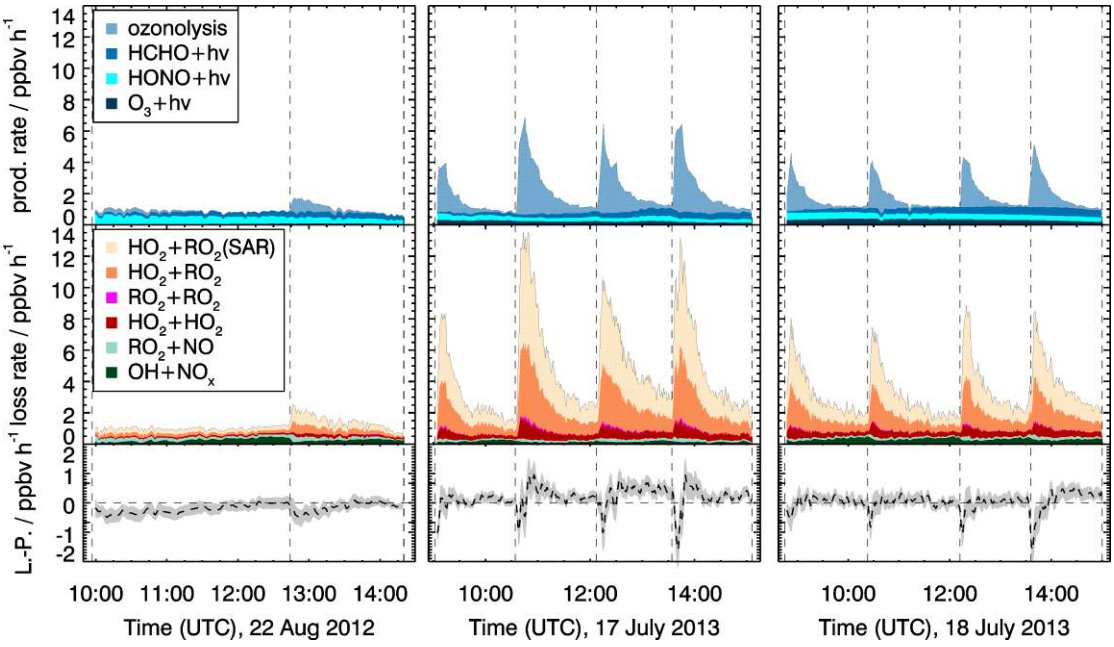

We revised the caption: "ROx primary production, P , (upper panels), termination L (middle panels) rates and their difference (lower panels). The rate constant of the reaction of MyO2 with HO2 was adjusted, to minimize the difference between radical production and destruction (see text for more explanation). The HO2 +RO2 (SAR) shows the additional radical loss if the unadjusted reaction rate constant is applied. In the bottom row, the lines show the difference between radical destruction and production (L − P) with adjusted rate constant of the reaction of MyO2 with HO2. Grey areas in the lower panels give the uncertainty of L − P ."

Pages 17-18, lines 528-530: The authors provide a sensitivity study to show the impact of additional MyO2 isomerization reactions on the production and loss of RO2 radicals in Figs. 11 and 12, producing one HOx radical for each isomerization reaction (line 529). How does the addition HOx production impact the OH and HO2 radical budgets in Figs.11 and 12? Does it improve the radical balance or make it worse?

We added in Line 529 to discuss the potential impact on the OH and HO_2 radical budget: "Because the yield of OH and HO_2 from potential isomerization and decomposition reactions of MyO_2 is not known, an upper limit of one OH and one HO_2 radical for each isomerization reaction is applied." In Line 534 we added: "Similar as for the RO_2 loss rate, potential production of OH and HO_2 from MyO_2 isomerization reactions would overcompensate the imbalances in their production and destruction rates."

Figures 11 and 12 are updated to show the maximum impact of OH and HO_2 production from isomerization reactions of MyO_2.

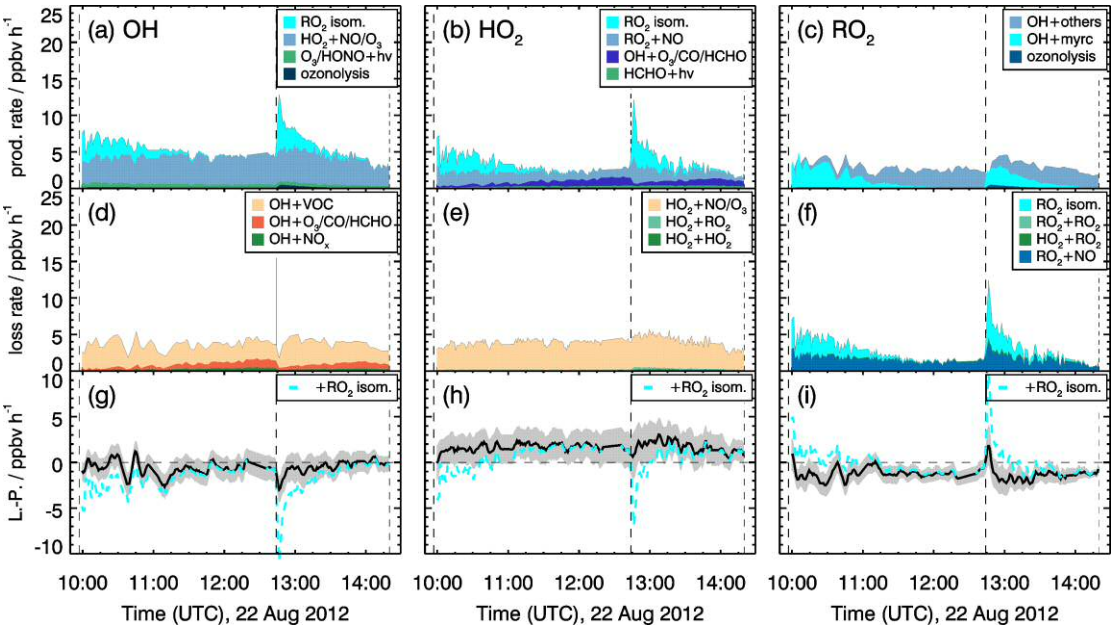

Revised Figure 11

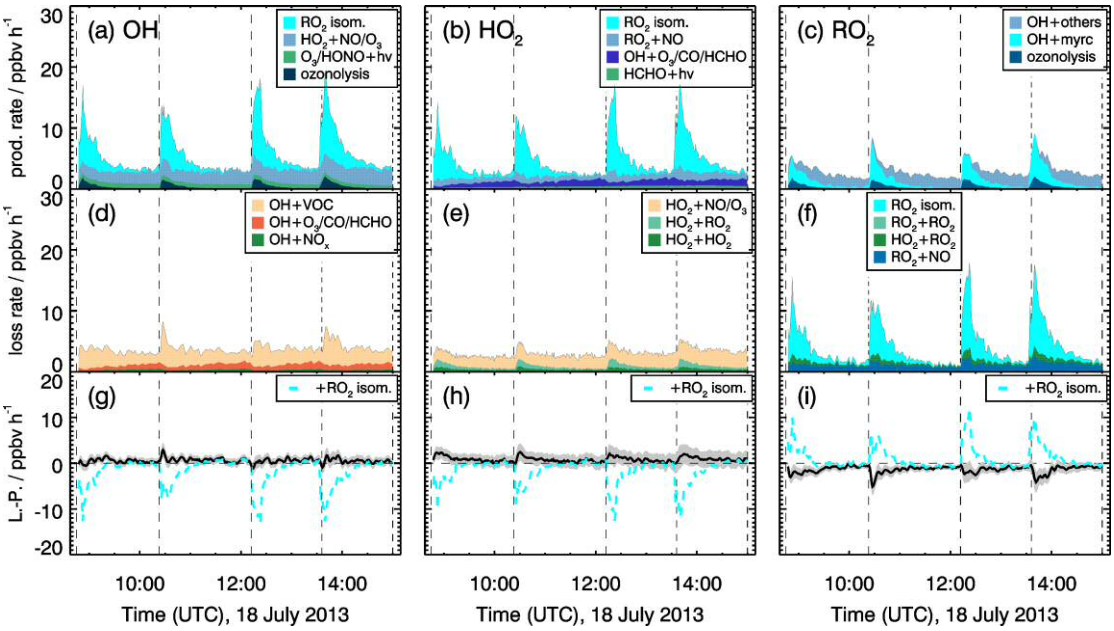

Revised figure 12

The captions are extended: "Upper limits for yields of OH and HO_2 radicals from MyO_2 isomerization reactions of one are assumed in the calculations of their production rates."

Atmospheric photo-oxidation of myrcene: OH reaction rate constant, gas phase oxidation products and radical budgets

Zhaofeng Tan[1], Luisa Hantschke[1], Martin Kaminski[1,a], Ismail-Hakki Acir[1,b], Birger Bohn[1], Changmin Cho[1], Hans-Peter Dorn[1], Xin Li[1,c], Anna Novelli[1], Sascha Nehr[1,d], Franz Rohrer[1], Ralf Tillmann[1], Robert Wegener[1], Andreas Hofzumahaus[1], Astrid Kiendler-Scharr[1], Andreas Wahner[1], and Hendrik Fuchs[1]

[1]Institute of Energy and Climate Research, IEK-8: Troposphere, Forschungszentrum Jülich GmbH, Jülich, Germany
[a]now at: Federal Office of Consumer Protection and Food Safety, Department 5: Method Standardisation, Reference Laboratories, Resistance to Antibiotics, Berlin, Germany
[b]now at: Institute of Nutrition and Food Sciences, Food Science, University of Bonn, Bonn, Germany
[c]now at: State Key Joint Laboratory of Environmental Simulation and Pollution Control, College of Environmental Sciences and Engineering, Peking University, Beijing, China
[d]now at: European University of Applied Sciences, Brühl, Germany

Correspondence: Hendrik Fuchs (h.fuchs@fz-juelich.de)

Abstract. The photo-oxidation of myrcene, a monoterpene species emitted by plants, was investigated at atmospheric conditions in the outdoor simulation chamber SAPHIR. The chemical structure of myrcene consists of one moiety that is a conjugated π-system (similar to isoprene) and another moiety that is a triple-substituted olefinic unit (similar to 2-methyl-2-butene). Hydrogen shift reactions of organic peroxy radicals (RO_2) formed in the reaction of isoprene with atmospheric OH radicals are known to be of importance for the regeneration of OH. Structure-activity relationships (SAR) suggest that similar hydrogen shift reactions like in isoprene may apply to the isoprenyl part of RO_2 radicals formed during the OH oxidation of myrcene. In addition, SAR predicts further isomerization reactions that would be competitive with bi-molecular RO_2 reactions for chemical conditions that are typical for forested environments with low concentrations of nitric oxide. Assuming that OH peroxy radicals can rapidly interconvert by addition and elimination of O_2 like in isoprene, bulk isomerization rate constants of $0.21\,s^{-1}$ and $0.097\,s^{-1}$ ($T = 298\,K$) for the 3 isomers resulting from the 3'-OH and 1-OH addition, respectively, can be derived from SAR. Measurements of radicals and trace gases in the experiments allowed to calculate radical production and destruction rates, which are expected to be balanced. Largest discrepancies between production and destruction rates were found for RO_2. Additional loss of organic peroxy radicals due to isomerization reactions could explain the observed discrepancies. The uncertainty of the total radical (RO_x=OH+HO_2+RO_2) production rates were high due to the uncertainty in the yield of radicals from myrcene ozonolysis. However, results indicate that radical production can only be balanced, if the reaction rate constant of the reaction between hydroperoxy (HO_2) and RO_2 radicals derived from myrcene is lower (0.9 to $1.6 \times 10^{-11}\,cm^3 s^{-1}$) than predicted by SAR. Another explanation of the discrepancies would be that a significant fraction of products (yield: 0.3 to 0.6) from these reactions include OH and HO_2 radicals instead of radical terminating organic peroxides. Experiments also allowed to determine the yields of organic oxidation products acetone (yield: 0.45 ± 0.08) and formaldehyde (yield: 0.35 ± 0.08). Acetone and formaldehyde are produced from different oxidation pathways, so that yields of these compounds reflect the branching ratios of the initial OH addition to myrcene. Yields determined in the experiments are consistent with branching ratios expected

from SAR. The yield of organic nitrate was determined from the gas-phase budget analysis of reactive oxidized nitrogen in the chamber giving a value of 0.13 ± 0.03. In addition, the reaction rate constant for myrcene + OH was determined from the measured myrcene concentration yielding a value of $(2.3 \pm 0.3) \times 10^{-10}\,\mathrm{cm^3 s^{-1}}$.

1 Introduction

Monoterpenes are emitted from vegetation accounting for approximately $160\,\mathrm{Tg}$ of the $1000\,\mathrm{Tg}$ of biogenic volatile organic compounds (VOCs) that are released into the atmosphere per year (Guenther et al., 2012; Sindelarova et al., 2014). Monoterpenes are highly reactive to the major oxidants in the atmosphere, hydroxyl radicals (OH), ozone (O_3) and nitrate radicals (NO_3) (Atkinson and Arey, 2003) and thus play an important role in ozone and secondary organic aerosol formation (Xu et al., 2015; Zhang et al., 2018; Schwantes et al., 2020).

Myrcene emissions contribute to the total biogenic monoterpene emissions in the range of 2 to 10 % (Guenther et al., 2012). Emission rates highly depend on the type of tree and season of the year (Helmig et al., 2013). In addition, there are hints for anthropogenic sources from the analysis of the composition of indoor air (Kostiainen, 1995). Few studies have been conducted to investigate the oxidation of myrcene (Deng et al., 2018; Atkinson, 1997; Reissell et al., 2002; Kim et al., 2011). In these studies, acetone, formaldehyde and $4-\mathrm{vinyl}-\mathrm{pentenal}$ have been identified as major oxidation products from the reaction of myrcene with OH, but yields determined in these studies vary. Lee et al. (2006) reported an organic nitrate yield of 10 % from the oxidation of myrcene by direct measurements using mass spectrometry. The reaction rate constant of myrcene + OH was determined to be $(2.1 \pm 0.2) \times 10^{-10}$ (Atkinson et al., 1986) and $(3.4^{+1.5}_{-1.0}) \times 10^{-10}$ (Hites and Turner, 2009) at room temperature with a discrepancy of up to 60 %. These results demonstrate the photo-oxidation of myrcene requires further investigation.

There is no detailed chemical mechanism of myrcene degradation by OH in literature. The acyclic structure of myrcene consists of two parts, an isoprenyl part ($CH_2{=}CH{-}C(={CH_2})CH_2-$ moiety) and another part that is structurally similar to $2-\mathrm{methyl}-2-\mathrm{butene}$ ($(CH_3)_2)C{=}CH{-}CH_2-$ moiety) (Fig. 1). Recent investigations of the oxidation of isoprene (Fuchs et al., 2013; Peeters et al., 2014; Wennberg et al., 2018; Novelli et al., 2020) revealed that organic peroxy radicals (RO_2) formed after the attack of OH to isoprene can rapidly interconvert, so that fast H-atom migration reactions of specific RO_2 isomers with initially low yield can significantly gain in importance. These reactions impact atmospheric chemistry most, if they become competitive with bi-molecular loss reactions such as reactions with nitric oxide (NO) and hydroperoxy radicals (HO_2). In the case of isoprene, these isomerization reactions can eventually regenerate OH radicals, so that a high OH regeneration efficiency of 0.5 can be sustained in the atmosphere also in regions, where radical termination reactions have been thought to dominate the fate of radicals (Novelli et al., 2020). Therefore, radical regeneration from isomerization reactions helped partly to explain observations of unexpectedly high OH concentrations in field experiments (Lelieveld et al., 2008; Hofzumahaus et al., 2009; Whalley et al., 2011). Radical regeneration from RO_2 isomerization reactions have also been shown to play a role in the oxidation of methacrolein (Fuchs et al., 2014; Crounse et al., 2012), 3-pentanone (Crounse et al., 2013), glyoxal (Lockhart et al., 2013), n-hexane, 2-hexanol (Praske et al., 2018), hydroxymethyl hydroperoxides (Allen et al., 2018), and 2-hydroperoxy-2-methylpentane (Praske et al., 2019).

In this study, the oxidation of myrcene by OH was investigated in the atmospheric simulation chamber SAPHIR (Simulation of Atmospheric Photochemistry In a Large Reaction Chamber) at Forschungszentrum Jülich. Experiments were performed under controlled conditions with concentrations of trace gases and radicals typical for atmospheric conditions. Experiments aim for adding to the determination of a degradation mechanism for myrcene.

2 Oxidation mechanism of myrcene

Myrcene is an acyclic hydrocarbon with three unsaturated carbon double bonds to which OH preferentially adds. One end of the myrcene molecule is structurally similar to isoprene and the other end is similar to 2-methyl-2-butene (Fig. 1). The myrcene oxidation by OH forms ten isomers of peroxy radicals ($\mathrm{MyO_2}$) (Fig. 2). Structure-activity relationships (SAR) by Peeters et al. (2007) suggest that OH preferably adds to the double bound of the isolated $-\mathrm{CH{=}C(CH_3)_2}$ moiety producing two peroxy radical species with yields of 17 % (7-OH-6-OO radical) and 31 % (6-OH-7-OO radical) (Fig. 2). When OH adds to the conjugated carbon double bonds, six isomeric hydroxy peroxy radicals are formed like in the OH or $\mathrm{NO_3}$ oxidation of isoprene (Peeters et al., 2009, 2014; Vereecken et al., 2021a). Addition to the $\mathrm{C_{3'}}$ position yields two allyl-like hydroxy radical isomers producing E-3'-OH-1-OO, 3'-OH-3-OO and Z-3'-OH-1-OO peroxy radicals after the subsequent addition of $\mathrm{O_2}$. A total yield of 31 % is estimated by SAR (Peeters et al., 2007) for these three isomers. Similarly, OH addition to the $\mathrm{C_1}$ position followed by addition of $\mathrm{O_2}$ to the allyl radical structure leads to the formation of E-1-OH-3'-OO, 1-OH-2-OO and Z-1-OH-3'-OO radicals with a total yield of 17 %. In the isoprene mechanism developed by Peeters et al. (2009, 2014); Novelli et al. (2020); Vereecken et al. (2021a), a central element is the fast interconversion reactions between the OH-adducts and corresponding OH peroxy radicals that proceed by addition and elimination of $\mathrm{O_2}$. Similar reactions are expected for the isoprene structure in myrcene (Fig. 2) establishing a coupled equilibrium between $\mathrm{MyO_2}$ isomers.

For OH attack on the $\mathrm{C_2}$ or $\mathrm{C_3}$ position of myrcene, the resulting OH adducts are not resonance stabilized and are hence not as favorable as the allylic-type radicals produced from $\mathrm{C_1}$ or $\mathrm{C_{3'}}$ addition. Yields of these $\mathrm{MyO_2}$ radicals are expected to be less than 2 % and therefore the chemistry of these two minor isomers is not further discussed in this work.

All $\mathrm{MyO_2}$ isomers can undergo bi-molecular reactions with NO, $\mathrm{HO_2}$ and other $\mathrm{RO_2}$ species. Specific reaction rate constants have not been measured, but values are expected to be within the range of typical rate constants for organic peroxy radicals. For example, SAR by Jenkin et al. (2019) suggests a value of $2.2 \times 10^{-11}\,\mathrm{cm^3 s^{-1}}$ ($T = 298\,\mathrm{K}$) of the reaction rate constants for the reaction of monoterpene derived $\mathrm{RO_2}$ (including $\mathrm{MyO_2}$) with $\mathrm{HO_2}$. Reaction products of the reaction of $\mathrm{RO_2}$ with $\mathrm{HO_2}$ are expected to be organic peroxides.

The reaction of the 6-OH-7-OO and 7-OH-6-OO radicals with NO produce mainly 4-vinyl-4-pentenal, acetone and $\mathrm{HO_2}$ (Fig. 3) as shown in experimental studies (Orlando et al., 2000; Reissell et al., 2002; Lee et al., 2006) as well as predicted by SAR (Vereecken and Peeters, 2009, 2010). Reissell et al. (2002) and Lee et al. (2006) suggested additional pathways for the alkoxy radical that is formed in the reaction with NO of these two $\mathrm{MyO_2}$ species. These pathways would include rearrangement reactions followed by reaction with NO and fragmentation. This was suggested to explain the observation of organic species with various masses (m/z=71, m/z=113, m/z=115) detected by the PTR-MS instrument in Lee et al. (2006).

Similarly, Böge et al. (2013) suggested a reaction pathway of 6-OH-7-OO and 7-OH-6-OO radicals to explain observed terpenylic acid in their experiments. The reaction of the other two most abundant radicals, 1-OH-2-OO and 3'-OH-3-OO, with NO would lead to the formation of HO_2 and formaldehyde together with 2-methyldiene-6-methyl-5-heptenal and 1-vinyl-5-methyl-4-hexanone, respectively (Fig. 3).

In addition to bi-molecular reactions, uni-molecular can be of importance for specific MyO_2. Due to the similarity of the conjugated double bond structure in myrcene and isoprene, it can be expected that H-shift reactions found to be important in isoprene (Peeters et al., 2009, 2014; Fuchs et al., 2013; Wennberg et al., 2018; Novelli et al., 2020) apply for corresponding MyO_2 radicals. Therefore, Z-3'-OH-1-OO and Z-1-OH-3'-OO radicals are expected to undergo α-OH 1,6-H migration followed by O_2 addition leading to hydroperoxy peroxy radicals (Fig. 4). As a first approximation, reaction rate constants can be assumed to be in the order of $1\,s^{-1}$ at 298 K like for corresponding reactions in isoprene (Peeters et al., 2014). Similar products from further isomerization and decomposition reactions could be expected as predicted for isoprene (Peeters et al., 2014). This would also lead to the regeneration of HOx radicals.

According to SAR by Vereecken and Nozière (2020), E-3'-OH-1-OO undergo an allylic 1,7 H-shift (Fig. 4). The reaction rate constant is estimated by this SAR to be high with a value of $8\,s^{-1}$ ($T = 298\,K$). In addition, E-1-OH-3'-OO can undergo an allylic 1,6 H-shift isomerization reaction with a fast isomerization reaction rate constant of $2\,s^{-1}$ ($T = 298\,K$). Products likely undergo fast ring-closure reactions on the dimethyl double bond with rates on the order of $1\,s^{-1}$ (pers. comm. Vereecken , 2021b).

As a consequence of the equilibration between different MyO_2 isomers that originate from the 3'-OH or 1-OH addition, a significant fraction of the MyO_2 can be removed through the H-shift reaction channels, if rates of competing bi-molecular reactions of all RO_2 isomers are low enough. In order to estimate effective bulk MyO_2 isomerization reaction rates, the distribution of MyO_2 isomers is estimated by using reaction rate constants for the oxygen addition and elimination reactions recommended for isoprene (Novelli et al., 2020). This results in a total bulk MyO_2 loss rate of approximately $0.21\,s^{-1}$ and $0.097\,s^{-1}$ ($T = 298\,K$) for the 3 isomers resulting from the 3'-OH and 1-OH addition, respectively. This means that isomerization reactions are becoming competitive for nearly half of the total MyO_2 (Fig. 2) isomers for chemical conditions with NO mixing ratios lower than 1 ppbv. It is worth noting that isomerization reactions rate constants have a strong temperature dependence, so that their impact can be significantly enhanced at higher temperatures. However, all rate constants by SAR predictions have also a high uncertainty of at least a factor of two and the uncertainty might be as high as a factor of 10 (Vereecken and Nozière, 2020).

3 Methods

3.1 Experiments in the SAPHIR chamber

The experiments were conducted in the outdoor atmospheric simulation chamber SAPHIR. SAPHIR has a cylindrical shape with double walls made of Teflon (FEP) film (length: 18 m diameter: 5 m, volume: $270\,m^3$). The space between the double walls is permanently purged with clean air to avoid diffusion of impurities from ambient air into the inner chamber. The walls

are transmissive for the entire solar UV and visible spectrum. The chamber is operated with synthetic air that is produced from evaporated liquid nitrogen and oxygen of highest purity (Linde, purity$>99.99990\,\%$). It is kept at a slight overpressure of $35\,\mathrm{Pa}$ that is maintained by a replenishment flow, which compensates for leakages and the sampling flow of analytical instruments. As a consequence, trace gases are diluted with a rate constant that is equivalent to a lifetime of approximately 17 hours. The air in the chamber can be exposed to sunlight by opening a shutter system. When the chamber film is exposed to solar radiation, nitrous acid (HONO), formaldehyde and acetone are released. The source strengths range between 100 to $200\,\mathrm{pptv/h}$. The photolysis of HONO leads to a continuous increase of nitrogen oxide concentrations in the chamber and is a significant source for hydroxyl radicals (OH). More details of the SAPHIR can be found in previous publications (e.g. Bohn et al., 2005; Rohrer et al., 2005).

In total 4 experiments investigating the oxidation of myrcene by OH were performed (Table 1), two of which were done at medium levels of nitric oxide (NO) ranging from 0.1 to 0.4 ppbv(18 August 2012: 0.18 to 0.43 ppbv NO (Fig. 5) and 22 August 2012: 0.15 to 0.30 ppbv of NO (Fig. S1 Supplement)) while lower NO mixing ratios below 0.11 ppbv were achieved in the other two experiments (17 July 2013, Fig. S2 Supplement, and 18 July 2013, Fig. S3 Supplement).

The experimental procedure was similar in all experiments. The chamber was cleaned in the night before the experiment by flushing the chamber with a high flow of synthetic air to remove all trace gases from previous experiments. Figure 5 shows, as an example, time series of trace gases for the experiment conducted on 22 August 2012. Experiments started in the morning with humidification of the chamber air in the dark. This was achieved by flushing evaporated Milli-Q water into the chamber together with a high flow of synthetic air. The chamber air was exposed to sunlight approximately for 1 hour without the presence of any additional reactant to determine the source strengths of chamber sources for formaldehyde for the specific experiment. In the experiments in 2013, approximately 50 ppbv ozone produced by a silent discharge ozonizer (O3onia) was injected to suppress NO in the reaction with O_3. Products from the ozonolysis of myrcene are similar to the products formed from the reaction with OH. These could lead to systematic errors in the conclusions with respect to the OH oxidation scheme. Given the typical OH concentration in this study ($5\times10^6\,\mathrm{cm^{-3}}$), the contribution of ozonolysis to the entire oxidation of myrcene is less than 20 %. The potential interfering is minimized in the medium NO cases, where ozonolysis only contributes 10 % of the myrcene oxidation.

Air mixtures of myrcene (Sigma-Aldrich, purity 99 %) were premixed in a canister (stainless steel with Silconert coating). The mixture was injected into the chamber air by calibrated mass flow-controllers to reach myrcene mixing ratios of several ppbv. Injections were done 2 times (approximately 2 ppbv each) in experiments with medium NO and four injections with smaller concentrations (approximately 1 ppbv) were done in the other experiments.

Additional reference experiments were performed using the same procedure like for the experiments with myrcene, but either with one injection of 140 ppmv of methane (29 May 2020 (Fig. S4 Supplement) and 10 July 2013) or three injections of 8.5 ppbv of α-pinene (03 September 2019 (Fig. S5 Supplement)). These experiments were used to evaluate the accuracies of the procedures that were used to analyse the organic nitrate formation and radical budgets in the experiments with myrcene.

3.2 Measurement of trace gas concentrations

Table 2 summarizes properties of instruments used in this work. The set of instruments was similar like used in previous experiments investigating the photochemistry of organic compounds (Kaminski et al., 2017; Fuchs et al., 2018; Novelli et al., 2018; Rolletter et al., 2019). Therefore, only a brief description is given here. Ozone was detected by a UV photometer (Ansyco). NO concentrations were measured by a chemiluminescence instrument (Eco Physics) that also detected nitrogen dioxide (NO_2) after conversion to NO in a photolytic converter. Methane, water vapour and carbon monoxide concentrations were measured by a cavity ring-down instrument (Picarro). Nitrous acid (HONO) was detected by a custom-built long-path absorption photometry (LOPAP) (Li et al., 2014). Photolysis frequencies were derived from solar actinic flux measurements by a spectroradiometer outside the chamber. Calculations take into account the reduction of radiation by the chamber construction elements and the Teflon film (Bohn and Zilken, 2005).

Myrcene was detected by gas chromatography coupled with a flame ionization detector (GC-FID) (Wegener et al., 2007) and by a proton-transfer-reaction mass-spectrometer (PTR-MS, Ionicon). The PTR-MS instrument was not calibrated for myrcene. Therefore, the signal was scaled to match the GC-FID measurements and used because of its higher time resolution (40 s) compared to that of GC-FID (30 min). Acetone and acetaldehyde were also measured by GC-FID. Formaldehyde (HCHO) measurements were performed by a Hantzsch instrument (AeroLaser) or by differential optical absorption spectrometry (DOAS). The HCHO concentrations measured by the different methods has been shown to agree within 10 % in a series of experiments in the SAPHIR chamber, in which both instruments concurrently measured (Glowania et al., 2020). OH reactivity (k_{OH}), which is the pseudo first-order rate constant of the OH radical loss, was measured by a laser flash photolysis - laser induced fluorescence instrument (Lou et al., 2010; Fuchs et al., 2017).

3.3 Measurement of radical concentrations

Measurements of OH radicals were performed by differential optical absorption spectrometry (DOAS) (Dorn et al., 1995) and laser-induced fluorescence (LIF) (Tan et al. (2017) and references therein). The DOAS instrument was not available in the experiment on 16 August 2012. In the experiment 6 days later (22 August 2012), OH concentrations measured by the LIF instrument were consistently 20 % higher than those measured by DOAS that is considered to be an absolute standard. The difference is larger than the combined 1σ uncertainty (14.5 %) of the measurements and is probably caused by a calibration error of the LIF instrument. This assumption is supported by the observed decay of myrcene which is caused by the reaction with OH. The decay can be accurately described with LIF data if these are reduced by 20 % in both experiments (Fig. S6 Supplement, Section 6.1). Therefore, OH measurements by LIF were scaled by a factor of 0.8 for both experiments. For the experiments in 2013, OH measurements by LIF and DOAS well agreed within 5 %. For the analysis of this work, OH measurements by the DOAS instrument are used if available. Interference could occur in OH measurements by ~~LIF~~ the LIF instrument from alkene ozonolysis (Fuchs et al., 2016) ~~, while~~ at exceptionally high concentrations of reactants (Fuchs et al., 2016) . However, the ozone and myrcene concentrations used in this study ~~was too low to yield a significant interference. If the Interference was related to alkene ozonolysis, it would be more severe in the experiments conducted in 2013 with higher O3,~~

were much lower compared to concentrations used in the characterization experiments in ~~contrast to the observations~~Fuchs et al. (2016). Therefore, it is not expected that similar interferences were significant for measurements in these experiments. Thus, the ~~difference in the OH measurements was~~ observed differences in the OH measurements of the LIF and DOAS instruments were most likely caused by calibration errors.

In addition to OH, peroxy radicals (HO_2 and RO_2) can be detected by the LIF instrument after chemical conversion to OH. The conversion of HO_2 radicals is accomplished by adding excess NO in a second low-pressure fluorescence cell, in which the sum of HO_2 and OH concentrations is measured (Fuchs et al., 2011). The measurement of RO_2 is accomplished in a 2-stage system (ROxLIF) in which all atmospheric RO_x radicals are first converted to HO_2 by added NO and CO in a flow reactor (Fuchs et al., 2008). This is followed by HO_2 to OH conversion with additionally added NO in a fluorescence cell. In this case, RO_2 is determined as the difference of RO_x and OH + HO_2. The operational parameters of the reactor are optimized to maximize the detection sensitivity for methyl peroxy radicals (CH_3O_2). However, it was found in previous studies that specific RO_2 species from other VOCs may be converted less efficiently in the reactor, if their conversion to HO_2 needs more reaction steps and therefore more reaction time than in case of CH_3O_2 (Fuchs et al., 2008). Alternative explanation for the lower sensitivity could be caused by the reversibility of the MyO_2 formation at low O_2 in the reactor, which slow down the conversion to HO_2.

For the evaluation of data in this work, the ROxLIF instrument was calibrated for CH_3O_2 and myrcene RO_2 radicals (MyO_2) that were produced by reaction of OH with the corresponding VOC in the radical calibration source as described by Fuchs et al. (2008). The detection sensitivity was only half as high for MyO_2 compared to CH_3O_2. The lower sensitivity could hint that some specific MyO_2 isomers are not efficiently converted to HO_2 for conditions inside the conversion reactor. The difference in the detection sensitivity for MyO_2 and other RO_2 species like CH_3O_2 adds to the uncertainty of measurements, because a mixture of different peroxy radicals is present during the experiments and the exact distribution of RO_2 species is not known. For the analysis in this work, the fraction of MyO_2 is estimated as described in the next subsection, in order to account for the lower sensitivity.

3.4 VOC reactivity and RO_2 speciation in myrcene experiments

The total OH reactivity (k_{OH}) that was measured in the experiments consists of reactivity from organic and inorganic compounds. Total OH reactivity was measured by LP-LIF while the speciated OH reactivity for individual species X was calculated from the products of concentrations of X and its reaction rate versus OH.The reaction of OH with most of the organic compounds leads to the formation of RO_2 radicals. Therefore, it is useful to distinguish between OH reactivity from those compounds unmeasured (k_{OHVOC}) and OH reactivity calculated from measured concentrations of inorganic compounds (CO, NO, NO_2) and formaldehyde:

$$k_{OHVOC} = k_{OH} - (k_8[HCHO] + k_9[CO] + k_{12}[NO_2] + k_{13}[NO]) \quad (1)$$

k_i are bimolecular rate constants of reactions R_i listed in Table 3. For the reference experiment with methane, only methane contributed to the VOC reactivity, because its oxidation product is formaldehyde, which does not produce RO_2 in the reaction with OH. Therefore, methyl peroxy radicals are the only RO_2 radical expected in that experiment. For the experiments with myrcene, the VOC reactivity includes the reactivity from myrcene and from partly unmeasured oxygenated organic compounds (OVOC) that are products of the myrcene oxidation. The OH reactivity from myrcene ($k_{\mathrm{OHmyrcene}}$) can be calculated from measured myrcene concentrations and the rate constant of its reaction with OH (k_7, Table 3):

$$k_{\mathrm{OHmyrcene}} = \mathrm{k_7[myrcene]} \tag{2}$$

Assuming that each OH reaction with an organic compound except formaldehyde in the experiments in this work leads to the formation of one RO_2 radical and all RO_2 radicals have similar chemical lifetimes, the distribution of RO_2 species from different VOCs is similar to the distribution of the OH reactivity from the VOCs. Therefore, the concentration of RO_2 derived from myrcene (MyO_2) can be approximated by scaling the total measured organic peroxy radical concentration ($[RO_2]_m$) that is determined assuming the same instrument sensitivity for all RO_2 with the ratio of OH reactivity from myrcene ($k_{\mathrm{OHmyrcene}}$) to the total OH reactivity from VOCs (k_{OHVOC}). Taking also into account that the sensitivity of the instrument for MyO_2 ($S_{\mathrm{MyO_2}}$) is reduced compared to the sensitivity for CH_3O_2 (S_{CH3O2}), the concentration of MyO_2 can be calculated from observed quantities:

$$[\mathrm{MyO_2}] = \frac{1}{\frac{S_{\mathrm{MyO2}}}{S_{\mathrm{CH3O2}}} + \frac{k_{\mathrm{OHVOC}}}{k_{\mathrm{OHmyrcene}}} - 1}[\mathrm{RO_2}]_m \tag{3}$$

RO_2 species originating from other hydrocarbons than myrcene ($RO_{2,\mathrm{other}}$) can be calculated using the remaining fraction of the VOC reactivity:

$$[\mathrm{RO_{2,other}}] = [\mathrm{MyO_2}]\left(\frac{k_{\mathrm{OHVOC}}}{k_{\mathrm{OHmyrcene}}} - 1\right) \tag{4}$$

Equations 3 and 4 allow calculating a more realistic total RO_2 concentration by taking the sum of MyO_2 and $RO_{2,\mathrm{other}}$ instead of using the measured RO_2 concentration, if the same instrument sensitivity for all RO_2 is assumed. An example of the result of this calculation is shown in Fig. 5 demonstrating that MyO_2 was the dominant RO_2 species right after each myrcene injection. However, these values have a high uncertainty that cannot easily be quantified, because, for example, the detection sensitivity for RO_2 produced in the reaction of OH with oxidation products may also differ from that of methyl peroxy radicals. The uncertainty of calculated RO_2 concentrations is lowest after each injection of myrcene, because the total OH reactivity and therefore RO_2 production is dominated by myrcene. Therefore, the analysis of radical production and destruction rates in this work (Section 6.4) focuses on the times right after each myrcene injection.

4 Experimental determination of organic nitrate yields

The determination of organic nitrate yields from photochemical VOC oxidation makes use of a budget analysis of the sum of NO_x and HONO in the chamber air. In the following, the sum of NO, NO_2 and HONO concentrations is defined as NO_y^*, which can be calculated from measurements of these species (Table 2).

In the sunlit SAPHIR chamber, the only source of reactive nitrogen is the emission of HONO from the chamber film (Section 3.1). The source strength $Q(\mathrm{HONO})$ is variable and depends on solar ultraviolet radiation, temperature and relative humidity (Rohrer et al., 2005). HONO is photolyzed to OH and NO (R1), which is further oxidized to NO_2 by reactions with O_3, HO_2 (Reaction R5), and RO_2 (Reaction R11). The sum of of NO_y^* is chemically lost in the chamber by reactions forming nitric acid (HNO_3) (Reaction R12) and organic nitrates ($RONO_2$) (R14). In addition, the NO_y^* species are removed ($L(NO_y^*)$) by transport due to the replenishment flow that compensates for chamber leakage and gas sampling of analytical instruments with a first-order rate constant of $k_d \approx 1.6 \times 10^{-5}\,\mathrm{s}^{-1}$ (Section 3.1):

$$L(NO_y^*) = ([NO] + [NO_2] + [HONO])\, k_d \tag{5}$$

The dilution rate is monitored by the input flow rate of synthetic air which yield an accuracy of k_d better than 1 %. Hence, the uncertainty due to the dilution is neglected due to its small contribution. The concentration of NO_y^* at a given time is then determined by the difference between the time-integrated production and loss terms.

$$[NO_y^*] = \int_t \left(Q(\mathrm{HONO}) - k_{12}[OH][NO_2] - k_{14}[RO_2][NO] - L(NO_y^*) \right) dt \tag{6}$$

It is assumed that the formation of HNO_3 and $RONO_2$ are effective sinks for NO_x and that reformation of NO_x by their reactions with OH or photolysis does not play a role. This assumption is justified because the low reaction rate constant with OH and small absorption cross sections of HNO_3 and $RONO_2$ (Burkholder et al., 2020; Browne et al., 2014) lead to their lifetimes in the range of several days, much slower than the time scale of the experiments. The loss of NO_2 due to reaction with ozone which forms nitrate radicals (NO_3) is neglected in Equation 6, because the NO_3 radical is efficiently converted back to NO_2 by photolysis and reaction with NO in the photo-oxidation experiments in this work. The formation of other oxidized nitrogen species such as peroxy nitric acid (HNO_4) and acetyl peroxy nitrate (PAN) is also assumed to be negligible because their mixing ratios are expected to be only a few tens pptv for conditions of the experiments.

The formation rate of HONO that is within the range of a few hundred $\mathrm{pptv/h}$ in the chamber experiments can be determined from measurements of OH, NO, HONO and j(HONO) by assuming a photo-stationary state for the HONO concentration:

$$\begin{aligned} \frac{d[\mathrm{HONO}]}{dt} &= Q(\mathrm{HONO}) - j_{\mathrm{HONO}}[\mathrm{HONO}] + k_{\mathrm{OH+NO}}[OH][NO] = 0 \\ Q(\mathrm{HONO}) &= j_{\mathrm{HONO}}[\mathrm{HONO}] - k_{13}[OH][NO] \end{aligned} \tag{7}$$

For the experimental conditions ($j(\mathrm{HONO}) = 8 \times 10^{-4}\,\mathrm{s}^{-1}$) photo-stationary state is reached within approximately 20 minutes. On this time scale, the dilution of HONO by the chamber replenishment flow is only 2 % and is therefore neglected. The uncertainty of the HONO formation rate (Equation 7 is dominated by the uncertainty in the HONO measurement (22 %, Table 3).

Using measured concentrations of NO, NO_2 and HONO, the concentration of NO that is converted to organic nitrates during the experiment ($\Delta\mathrm{RONO_2}$) is determined by the balance of nitrogen oxide concentrations:

$$\begin{aligned}
\Delta[\mathrm{RONO_2}] &= \int_t k_{14}[\mathrm{RO_2}][\mathrm{NO}]dt \\
&= \Phi_{\mathrm{RONO2}} \int_t (k_{11} + k_{14})[\mathrm{RO_2}][\mathrm{NO}]dt \\
&= \int_t \left(Q(\mathrm{HONO}) - k_{12}[\mathrm{OH}][\mathrm{NO_2}] - L(\mathrm{NO_y^*})\right) dt - ([\mathrm{NO}] + [\mathrm{NO_2}] + [\mathrm{HONO}])
\end{aligned} \tag{8}$$

The reaction yield of organic nitrates (Φ_{RONO2}) can be then derived as slope of a linear fit (Equation 8). The accuracy of the yield is mainly determined by the accuracy the kinetic reaction rate constants and measurements that vary between the specific experiments.

4.1 Test experiments with methane and α-pinene

In order to test the method described above, organic nitrate yields from the photo-oxidation of methane and α-pinene were experimentally determined and compared with literature values. NO mixing ratios were between 100 to 300 pptv in both experiments, so that at least 60 % of the RO_2 radicals reacted with NO.

Figure 6 shows time series of NO_y species in α-pinene and methane experiments. In the methane experiment, the total mixing ratio of NO_y species calculated from the HONO chamber source (Equation 7) is around 1.3 ppbv and is mainly explained by measured NO_2 and NO concentrations. In the experiment with α-pinene, the calculated NO_y mixing ratio increased from 1 to 1.3 ppbv within two hours. Approximately 1 ppbv was present as NO_2 and NO and the remaining fraction can be attributed to the formation of organic nitrates from α-pinene. The alkyl nitrate yield is derived from Equation 8 by a linear fit as described above.

For the experiment with methane, the alkyl nitrate yield is smaller than error of the calculation (0.00 ± 0.04, Fig. 6). This small value agrees with literature values of < 0.003 (Scholtens et al., 1995) and 0.0039 ± 0.0011 (Butkovskaya et al., 2012) at room temperature.

The alkyl nitrate yield determined from the OH oxidation experiment with α-pinene is 0.32 ± 0.06. The accuracy is mainly due to the uncertainty of RO_2 measurements. Reported literature values are 0.01 (Aschmann et al., 2002), 0.18 ± 0.09 (Noziére et al., 1999) and 0.26 ± 0.07 (Rindelaub et al., 2015). All experiments were conducted at measurement conditions where the reaction of RO_2 with NO was the dominant RO_2 reaction pathway, so that the obtained organic nitrate yields can be attributed to the yield from reaction of α-pinene derived RO_2. The value determined in this work agrees well with values determined from direct measurements using FT-IR spectroscopy in experiments by Noziére et al. (1999) and Rindelaub et al. (2015) within

the specified errors. In contrast, Aschmann et al. (2002) approximated the nitrate yield from mass spectrometer measurements with a high uncertainty that likely explains the much lower yield in their experiments compared to the other two studies and results in this work.

The good agreement between nitrate yields determined in the experiments with methane and α-pinene with reported values in literature demonstrates that the applied method for the determination of alkyl nitrate formation in the chamber gives reliable results.

5 Experimental analysis of the chemical budgets of OH, HO_2, RO_2 and RO_x

The chamber experiments are also used to study the chemical budgets of OH, HO_2, RO_2, and RO_x during the photochemical oxidation of myrcene. Radical production and destruction rates are determined from reaction kinetic data and measured trace gas concentrations for reactions that are known to produce or consume radicals in the experiments. Because the chemical lifetime of radicals is short (seconds to minutes), the radical concentrations are expected to be in steady state. Therefore, the total loss rates for each radical species is balanced by its total production rate. Analysing radical production and destruction rates using experimental data gives an indication if reactions taken into account can describe observations or if there are contributions from further reactions. A similar method has been used before by Tan et al. (2019, 2020) to analyse radical budgets in atmospheric air in China. Here, the method is tested for the photochemical degradation of methane and then applied to the more complex degradation mechanism of myrcene.

5.1 Radical production, destruction and regeneration reactions

In the chamber experiments, OH, HO_2 and RO_2 radicals are primarily formed from photolysis of HONO (Reaction R1), O_3 (Reaction R2), formaldehyde (Reaction R3), and from the ozonolysis of myrcene (Reaction R4). Radical termination processes include the formation of nitrates (HNO_3, HONO and $RONO_2$, Reactions R12, R13 and 14) and peroxides (ROOH and H_2O_2, Reaction R15 and R16). The contribution from RO_2 self-combination reactions is neglibile and not considered here. The photolysis of peroxides that can lead to the production of radicals is neglected due to the slow photolysis frequency (typical value for example for CH_3OOH: $2 \times 10^{-6}\,s^{-1}$ at noontime). The rates for the primary production of RO_x radicals ($P(\mathrm{ROx})$) and for the termination loss rate ($L(\mathrm{ROx})$) can be calculated as:

$$P(\mathrm{RO_x}) = j_{\mathrm{HONO}}[\mathrm{HONO}] + \Phi_{\mathrm{OH},2} j_{\mathrm{O(^1D)}}[\mathrm{O_3}] + 2 j_{\mathrm{HCHO}}[\mathrm{HCHO}] + (\Phi_{\mathrm{OH},4} + \Phi_{\mathrm{RO_2},4}) k_4 [\mathrm{VOC}][\mathrm{O_3}] \quad (9)$$

$$L(\mathrm{RO_x}) = (k_{12}[\mathrm{NO_2}] + k_{13}[\mathrm{NO}])[\mathrm{OH}] + (k_{14}[\mathrm{NO}] + 2k_{15}[\mathrm{HO_2}])[\mathrm{RO_2}] + 2k_{16}[\mathrm{HO_2}]^2 \quad (10)$$

For the calculation of $P(\mathrm{RO_x})$ and $L(\mathrm{RO_x})$, measured radical and trace gas concentrations are used. For the analysis of the myrcene experiments, total RO_2 concentrations include corrections for the reduced detection sensitivity of MyO_2 as explained in Section 3.4. The applied rate constants are listed in Table 3. The OH and RO_2 yields are taken from Deng et al. (2018)~~, in which~~. In their work, the yield of HO_2 is zero. The lumped rate constant for the reactions between RO_2 and HO_2 (R15) has

a rather large uncertainty, because rate constants of different RO_2 species can be different by up to a factor of 4 (Jenkin et al., 2019). The uncertainty of other reaction rate constants is typically around 10 %. In addition, the accuracies of measurements (Table 2) add to the total uncertainty in the calculation of loss and production rates. In these experiments, there is a small background OH reactivity ($< 1\,s^{-1}$) which can be a permanent loss of radicals, but could also regenerate HO_2 and/or RO_2. However, this background reactivity is small compared to the OH reactivity from methane and myrcene during the experiments ($> 15\,s^{-1}$), so that it does not affect the analysis.

If production and destruction rates of single RO_x species (OH, HO_2 and RO_2) are calculated, radical conversion reactions need to be additionally taken into account. The total OH loss rate ($L(OH)$) can be quantified by the product of measured OH concentrations and total OH reactivity:

$$L(OH) = [OH]k_{OH} \tag{11}$$

The OH production rate ($P(OH)$) can be calculated from the sum of production from HONO (Reaction R1) and O_3 photolysis followed by water reaction (Reaction R2), ozonolysis of VOCs (Reaction R4) and radical regeneration from HO_2 reacting with NO (Reaction R5) or O_3 (Reaction R6):

$$P(OH) = j_{HONO}[HONO] + \Phi_{OH,2} j_{O(^1D)}[O_3] + \Phi_{OH,4} k_4[VOC][O_3] + (k_5[NO] + k_6[O_3])[HO_2] \tag{12}$$

The loss of HO_2 ($L(HO_2)$) and RO_2 ($L(RO_2)$) radicals are dominated by their reactions with NO for conditions of the experiments here (Reactions R5, R11, R14) in addition to recombination of peroxy radicals including reactions of HO_2 with RO_2 (Reaction R15) and HO_2 self-reactions (Reaction R16):

$$L(HO_2) = (k_5[NO] + k_6[O_3] + k_{15}[RO_2] + 2k_{16}[HO_2])[HO_2] \tag{13}$$

$$L(RO_2) = ((k_{11} + k_{14})[NO] + k_{15}[HO_2])\,[RO_2] \tag{14}$$

The HO_2 production ($P(HO_2)$) rate can be calculated from the photolysis of aldehydes, of which HCHO (Reaction R3) were measured in these experiments, and reactions that convert OH or RO_2 to HO_2. OH to HO_2 conversion occurs in the reaction of OH with HCHO (Reaction R6), CO (Reaction R7) and O_3 (Reaction R8). The reaction of RO_2 with NO (Reaction R9) produces either HO_2 or organic nitrates (Reaction R14). The total HO_2 production rate is then calculated as:

$$P(HO_2) = 2j_{HCHO}[HCHO] + (k_6[HCHO] + k_7[CO] + k_8[O_3])[OH] + k_{11}[NO][RO_2] \tag{15}$$

RO_2 primary production consists of the ozonolysis of VOCs (Reaction R4). In addition RO_2 is produced from radical propagation reactions via the reaction of OH with VOCs. The total production rate ($P(RO_2)$) can be calculated from the VOC reactivity, k_{OHVOC}, (Equation 1) assuming that each reaction of a VOC with OH produces one RO_2 radical:

$$P(\mathrm{RO_2}) = \Phi_{\mathrm{RO2}} k_4 [\mathrm{VOC}][\mathrm{O_3}] + \mathrm{k_{OHVOC}}[\mathrm{OH}] \quad (16)$$

5.2 Radical production and destruction in a test experiment with methane

The chemical radical budget analysis in SAPHIR experiments was tested in a photo-oxidation experiment with methane. The chemical oxidation mechanism of methane is much simpler than that of monoterpenes. (1) Ozonolysis reactions do not play a role. (2) Organic peroxy radicals that are formed in the chemical mechanism are methyl peroxy radicals ($\mathrm{CH_3O_2}$), which can be accurately measured by the ROxLIF system. (3) There are recommendations for rate constants for reactions involving methyl peroxy radicals (IUPAC, 2020).

Reaction rates for the methane oxidation experiment (29 May 2020) are shown in Fig. 7. Since no DOAS OH measurements were available for this experiment, OH measurements by the LIF instrument were used (Fig. S4). Total turnover rates are similar for all single radical species (OH, $\mathrm{HO_2}$, $\mathrm{RO_2}$) with values between 8 and 12 $\mathrm{ppbv/h}$ and do not vary much over the course of the experiment. The loss of peroxy radicals is dominated by the radical regeneration reaction with NO whereas radical recombination reactions contribute less than 10 % to the entire loss of peroxy radicals. OH is nearly only lost by its reaction with methane and formaldehyde.

The production and destruction rates of total $\mathrm{RO_x}$ are significantly smaller than those of single radical species with values that rise from 2 to 4 $\mathrm{ppbv/h}$ over the course of the experiment as radical regeneration reactions cancel out. The increase is due to radicals from the photolysis of formaldehyde that is continuously produced from the chamber wall (Section 3.1) and in the reaction of OH + methane. The increase in radical production is balanced by increasing rates of peroxy radical recombination reactions and of the reaction of OH with $\mathrm{NO_2}$. The latter is due to the increase of nitrogen oxide concentrations from the chamber source of nitrous acid.

Radical production and destruction rates of each radical species and of total $\mathrm{RO_x}$ are roughly balanced within the uncertainty of the calculation (Fig. 7). Maximum deviations are less than 0.5 $\mathrm{ppbv/h}$ for the production and destruction rates of $\mathrm{RO_x}$ and $\mathrm{HO_2}$. Differences are much smaller than the accuracy of the calculation (1.5 $\mathrm{ppbv/h}$ for $\mathrm{RO_x}$ and 2 $\mathrm{ppbv/h}$ for $\mathrm{HO_2}$). Higher deviations with values of up to 4 $\mathrm{ppbv/h}$ are seen for OH and $\mathrm{RO_2}$ but opposite behaviour. The accuracy of OH and $\mathrm{RO_2}$ radical production and destruction rates are in the range of 2 to 3 $\mathrm{ppbv/h}$, which cannot explain the discrepancies. As the $\mathrm{RO_x}$ and $\mathrm{HO_2}$ budget are closed using measured OH concentrations, the imbalance between OH and $\mathrm{RO_2}$ production and destruction indicates an unknown systematic error in the conversion rate from OH to $\mathrm{RO_2}$. One possible explanation for the observed imbalances would be that the calculated reaction rate of OH + $\mathrm{CH_4}$ is too large. This could either be caused by the measured OH or $\mathrm{CH_4}$ concentrations being too high, or by the applied reaction rate constant $k_{\mathrm{OH+CH_4}}$ being too large.

The methane concentrations in the chamber were above the measurement range specified by the manufacturer (Picarro, 0-20 ppmv. However, an instrumental test of the instrument done prior to the chamber experiment showed that the stated measurement accuracy holds at the concentrattion (150 ppmv) used in the presented experiment. A small background reacitivty of 2 $\mathrm{s^{-1}}$ was found before the injection of methane. The OH reactivity calculated from measured methane concentration and

the reaction rate constant is about $26\,s^{-1}$, which is consistent with the direct OH reactivity measurement considering the contribuion of background reactivity (Fig. S4). This gives the confidence on the accuracy of the methane measurement.

Another reason for the imbalances could be LIF calibration errors that are larger than given in Table 2. The specification for OH in Table 2 was generally confirmed in previous intercomparisons with the OH-DOAS instrument. However, in some instances the LIF measurements were found to deviate more than expected. An example are the experiments on 16 Aug and 22 Aug 2012 (Fig. 5 and Fig. S1), where the LIF measurements are higher than the DOAS data by a factor 1.2 probably due to an incorrect calibration.

In the following Section, radical budgets for the chemical degradation of myrcene are investigated. In these cases, also OH-DOAS data were available which have a generally better accuracy than LIF. Therefore, the DOAS data were used for the budget analysis (Fig. 10 - 12). Note that LIF and DOAS showed good agreement in these experiments (Fig. S2 and S3).

The rate constant for $OH + CH_4$ has an uncertainty factor of f=1.1 according to NASA/JPL (Burkholder et al., 2020) and f=1.15 according to IUPAC (Atkinson et al., 2004). Thus, 10-15% difference in the radical budgets would be explainable by a too large rate constant.

This partly unresolved discrepancy shows the limitation of the analysis of radical production and destruction rates and needs to be further investigated. The analysis of the experiment with the well-defined chemistry of methane indicates that the maximum accuracy of calculated differences between production and destruction rates for single radical species is 20 % in the chamber experiments.

6 Results and discussion of the experiments with myrcene

6.1 Reaction rate constant of the OH reaction with myrcene

The rate constant of the reaction of myrcene with OH is determined from the measured temporal decay of myrcene and the measured OH concentration. The time series of measured myrcene concentrations are compared to calculations using a chemical box model that only includes chemical loss reactions with OH and O_3 and dilution. The model is constrained to measured values of temperature, pressure, the dilution rate constant, OH and O_3 concentrations. The initial myrcene concentration is set to the injected amount of myrcene. The reaction rate constant for myrcene with O_3 is taken from the work by Kim et al. (2011) who measured a value of $2.21 \times 10^{-15} \exp(-(520 \pm 109)K/T)\,cm^3s^{-1}$ using relative rate technique. Atkinson et al. (1986) suggested a nearly 20 % faster reaction rate constant of $4.7 \times 10^{-16}\,cm^3s^{-1}$ ($T = 298\,K$) that is still consistent with the value by Kim et al. (2011) within the experimental uncertainties. The chemical lifetime of myrcene with respect to the ozonolysis reaction was approximately 44 min in the low NO_x experiments with O_3 concentrations of 40 ppbv but was up to 3 hours in the experiments with medium NO_x and O_3 concentrations of less than 10 ppbv. In comparison, the chemical lifetime of myrcene with respect to the reaction with OH was within the range of 15 min at OH concentrations of approximately $5 \times 10^6\,cm^{-3}$ observed in all experiments. Hence, the contribution of ozonolysis to the total chemical loss of myrcene in the experiments was 10 % to 26 %.

The rate constant of the reaction of myrcene with OH is optimized, such that the difference between measured and modelled myrcene concentration time series is minimized. For this optimization the OH concentration observed from DOAS is used. This procedure is applied to all three experiments resulting in a rate constant of $(2.3 \pm 0.3) \times 10^{-10}\,\mathrm{cm^3 s^{-1}}$ ($T = 298\,\mathrm{K}$, Table 4, Fig. S6 Supplement). The error results mainly from the variability of values determined in the different experiments.

The rate constant determined in this study is in good agreement with those reported in the literature (Table 4). Relative rate technique was used in experiments by Atkinson et al. (1986) and Grimsrud et al. (1975). The value reported by Hites and Turner (2009) ($3.4 \times 10^{-10}\mathrm{cm^3 s^{-1}}$) is higher than those of this work and reported by Atkinson et al. (1986), but has a high uncertainty of $\pm 35\,\%$ that is explained by experimental difficulties in the handling of myrcene. The reaction rate constants calculated from structure-activity relationship (SAR) by Peeters et al. (2007) and Jenkin et al. (2018) give similar results between of 1.8 to $1.9 \times 10^{-10}\mathrm{cm^3 s^{-1}}$. Values are approximately 20 % lower than the experimentally derived reaction rate constants. However, differences are within the accuracy of SAR predictions.

6.2 Product yields of the reactions of myrcene hydroxy peroxy radicals with NO

When OH reacts with myrcene, about half (48 %) of the OH adds to the $-\mathrm{CH{=}C(CH_3)_2}$ moiety and the other half (48 %) to the isoprenyl part (Peeters et al., 2007). In comparison, the SAR developed by Jenkin et al. (2018) predicts a branching ratio of 63:37 for OH addition to the $-\mathrm{CH{=}C(CH_3)_2}$ and the isoprenyl part, consistent with the values reported in (Peeters et al., 2007). In this work, the branching ratio is adapted from Peeters et al. (2007) to be consistent with other studies. In the first case, 4-vinyl-4-pentenal and acetone are formed from the reaction of $\mathrm{MyO_2}$ with NO (Section 2). In the second case, 2-methylidene-6-methyl-5-heptenal or 1-vinyl-5-methyl-4-hexenone are produced together with formaldehyde. Thus, the yields of acetone and formaldehyde are indicators for the yields of the OH addition to myrcene.

Acetone and formaldehyde yields are calculated from measured time series of product species and myrcene in the experiments on 16 and 22 August 2012, when NO mixing ratios were 200 pptv, so that >90 % of $\mathrm{RO_2}$ reacted with NO (Fig. 5). Only measurements after the first myrcene injection are used here to avoid that secondary chemistry impacts the yield determination. The two other experiments are not considered for three reasons. The large amount of ozone (up to 50 ppbv) would require considerable correction for myrcene ozonolysis. Second, due to the lower NO concentration, reactions of $\mathrm{RO_2}$ with $\mathrm{HO_2}$ would be competitive with the reaction of $\mathrm{RO_2}$ with NO. Third, the smaller amount of injected myrcene produced less oxidation products.

Corrections are applied to measured myrcene, formaldehyde and acetone time series, in order to relate myrcene that reacted with OH and product species that are chemically formed from this reaction following the procedure described in previous work (Galloway et al., 2011; Kaminski et al., 2017). Product concentrations are corrected for losses due to dilution, photolysis and reaction with OH. In addition, formation of formaldehyde and acetone from chamber sources need to be subtracted from the measured concentrations. Myrcene concentrations are also corrected for dilution and the fraction of myrcene that reacted with ozone. After corrections have been applied, the relationships between consumed myrcene and product concentrations are linear, if species are mainly formed as first-generation products in the reaction of myrcene and OH. The slopes give acetone

and formaldehyde yields of 0.45 ± 0.08 and 0.35 ± 0.08, respectively (Fig. 8). The error is caused by the uncertainty in the source strengths of chamber sources for acetone and formaldehyde and the accuracy of measurements.

The acetone yield is in excellent agreement with SAR predictions that 48 % of the OH adds to the double bond of the $-CH{=}C(CH_3)_2$ moiety (Peeters et al., 2007). The formaldehyde yield of 0.35 ± 0.08 is lower than the SAR prediction for the OH attack to the isoprenyl part (0.48). One possible reason for the smaller than expected formaldehyde yield could be isomerization reactions of the myrcene peroxy radicals shown (Fig. 3), which may not lead to the production of HCHO. The estimated bulk isomerization rates of $0.097\,s^{-1}$ and $0.21\,s^{-1}$ (Section 2) are sufficiently fast to compete with the loss rate of $0.04\,s^{-1}$ for MyO_2 with 200 pptv of NO, so that the reduced formaldehyde yield could be fully explained by isomerization reaction pathways. A different explanation for the lower formaldehyde yield compared to acetone is that the nitrate yield is larger for the MyO_2 that would otherwise end up as formaldehyde. In fact, the total product yields is closed to unity (acetone (0.45 ± 0.08) + formaldehyde (0.35 ± 0.08) + nitrate (0.13 ± 0.03) = 0.93 ± 0.12).

Acetone and formaldehyde yields agree with published results by Reissell et al. (2002) and Orlando et al. (2000) (Table 5). Lee et al. (2006) reported a smaller acetone yield of 0.22 ± 0.02 and a significantly higher HCHO yield of 0.74 ± 0.08. However, their HCHO yield carries a large uncertainty because concentrations were outside the range for which the instrument was calibrated.

The oxygenated organic compound 4-vinyl-4-pentenal has been detected in previous studies from the reaction of myrcene with OH (Reissell et al., 2002; Lee et al., 2006). Fragmentation in the PTR-MS and further oxidation of 4-vinyl-4-pentenal complicated the unambiguous yield determination. Therefore, Lee et al. (2006) reported a high yield of 0.4, but also state a lower limit of 0.09. Acetone is the co-product of 4-vinyl-4-pentenal (Fig. 3). The high limit yield of 0.4 for 4-vinyl-4-pentenal by Lee et al. (2006) is therefore consistent with the acetone yield determined in this work. The yield of 4-vinyl-4-pentenal was also measured by Reissell et al. (2002), but a lower yield of 0.19 ± 0.04 was found. This low yield is apparently inconsistent with the yield of 0.45 ± 0.06 for the co-product acetone determined in the same experiments (Table 5). The authors suggest that there could be re-arrangement of the hydroxyalkoxy radical that compete with the decomposition to 4-vinyl-4-pentenal, but may still lead to acetone production, so that the yield for acetone could become higher than that of 4-vinyl-4-pentenal.

The yield of organic nitrate from reactions of MyO_2 with NO is determined from the analysis of reactive nitrogen oxides in the chamber as described in Section 4. This results in an organic nitrate yield of 0.13 ± 0.03 (Fig. 9). This value is consistent with the yield of 0.10 ± 0.03 reported by Lee et al. (2006), who directly measured organic nitrates by mass spectrometry. Values are lower than the yield expected from SAR described in Jenkin et al. (2019), which predicts a yield of 0.19 that would also apply for other monoterpenes, but may still be within the uncertainty of the SAR predictions. Like for the formaldehyde yield, the smaller than predicted organic nitrate yield may also be partly due to competing MyO_2 isomerization reactions.

6.3 Primary radical production and termination

The primary radical production is due to photolysis (Reactions R1 to R3) and ozonolysis reactions (Reaction R4). Production rates by photolysis of O_3, HONO and HCHO are calculated using measured trace gas concentrations and photolysis frequencies. The calculation of the production rate from myrcene ozonolysis requires the knowledge of both the reaction rate constant

(Section 6.1) and the yield of OH and RO_2 radicals. The uncertainty of yields are high. Values range from 0.71 determined from high-level quantum chemistry calculations and kinetic calculations (Deng et al., 2018) to experimental values of 1.15 with an uncertainty of a factor of 1.5 (Atkinson et al., 1992). It is worth noting that additional radicals could be produced from ozonolysis reactions of oxidation products at later times of the experiment because first-generation organic products from the reaction of myrcene with OH still contain C−C double bonds that can react with ozone.

The radical termination reactions include reactions with nitrogen oxides (Reactions R12-R14) and radical self-reactions (Reactions R15, R16). Loss of radicals in the reaction with NO_x and the HO_2 self-reaction contribute less than 1 ppbv/h to the total loss rate each. Contributions from RO_2 self-reactions are expected to be negligible ($< 2\,\%$) because their reaction rate constants are typically much smaller than those of RO_2+HO_2 reactions (Table 3). The reaction rate constant of the MyO_2+HO_2 reaction is estimated from SAR by Jenkin et al. (2019) and therefore, the value could also have a high uncertainty.

In the experiment with medium NO concentrations (22 August 2012), the total radical production is low with values of less than 1.5 ppbv/h and radical production and destruction are balanced (Fig. 10). No ozone is added, so that radical production from ozonolysis plays a minor role, and radical loss by radical recombination is suppressed due to the competition of peroxy radical reactions with NO. Therefore, the uncertainties in the radical yield of myrcene ozonolysis and the reaction rate constant of the MyO_2+HO_2 reaction do not impact the results.

In contrast, radical production and destruction rates in experiments performed at low NO concentrations (17 July 2013, 18 July 2013) that is achieved by suppressing NO in the reaction with O_3 are dominated by radical production from myrcene ozonolysis and radical destruction by MyO_2+HO_2 reactions right after the injection of myrcene. Taking the upper limit of the radical yield from the ozonolysis reaction of 1.42 (0.71 for OH and 0.71 for MyO_2), the production is 4 ppbv/h. The radical primary production could be smaller, if the unspeficied radical yield of 1.15 suggested by Atkinson et al. (1992) is applied. Applying the reaction rate constant of the MyO_2+HO_2 derived by SAR (Section 2) results in a maximum radical loss rate of 13.5 ppbv/h also right after the injection of myrcene when MyO_2 concentrations are highest. Because this high destruction rate cannot be balanced by radical production, either the reaction rate constant must be lower than SAR predictions or there are reaction pathways that do not lead to radical termination products (organic peroxide), but regenerate radicals. Due to the high uncertainty of radical production from ozonolysis in these experiments, no firm conclusion can be drawn. The reaction rate constant suggested by Jenkin et al. (2019) would need to be reduced between a factor of 0.4 and 0.7 (0.9 to 1.6×10^{-11} cm^3s^{-1} ($T = 298$ K, Table 3) or the yield of of radical products would need to be in the range of 0.3 and 0.6 to match the range of radical production.

A reduced MyO_2+HO_2 reaction rate constant is significantly different from the SAR predictions by Jenkin et al. (2019). The SAR value is similar for all monoterpenes and well agrees with direct measurements for the reaction rate constant of HO_2 with RO_2 derived from α-pinene (2.1×10^{-11} cm^3s^{-1}), γ-terpinene (2.0×10^{-11} cm^3s^{-1}) and limonene (2.1×10^{-11} cm^3s^{-1}) reported by Boyd et al. (2003). A high yield of radical products from the MyO_2+HO_2 reaction may not be expected from analogies of isoprene and 2-methyl-2-butene (Liu et al., 2012; Paulot et al., 2009). For these reasons there is no clear conclusion, how exactly rate constants and yields need to be adjusted to balance the ROx production and destruction rates.

6.4 ROx radical chain propagation reactions

The total production and loss rates of OH, HO_2 and RO_2 radicals do not exhibit much variability over the course of the experiments with medium NO concentrations (Fig. 11, Fig. S7 Supplement). In the experiments with low NO, the turnover rates of radical production and destruction reactions for OH, HO_2, and RO_2 exhibit peak values when myrcene is injected (Fig. 12 and Fig. S8 Supplement). This distinct feature is related to the elevated radical production of up to 2 ppbv/h from the ozonolysis of myrcene and peak concentrations of peroxy radical concentrations.

Production and destruction rates of OH radicals are balanced within the accuracies of the calculation in all experiments. Rates are similar in all experiments with values around 4 ppbv/h. Maximum RO_2 turnover rates are lower (2 to 3 ppbv/h) compared to those of OH and HO_2, because up to 25 % of the OH radicals are directly converted to HO_2, for example in the reaction of OH with CO or HCHO. Because myrcene is consumed within a few hours, the turnover rate of RO_2 is decreasing over time after each myrcene injection. In experiments with medium NO concentrations, HO_2 radical production and destruction rates are not balanced by 0.5 of 1.5 ppbv/h in contrast to those of OH. Discrepancies, however, are only slightly larger than the 1-σ uncertainty of the calculated values. The total uncertainty is dominated by the accuracy of RO_2 measurements because of the low detection sensitivity of the instrument for MyO_2 and the uncertainty in the sensitivity of other RO_2 formed from oxidation products that are dominant, once myrcene reacted away.

Even higher discrepancies of up to 2 ppbv/h between HO_2 and RO_2 production and destruction rates are observed in the experiments with low NO mixing ratios. Values are highest right after each myrcene injection with the HO_2 production rate being lower than the destruction rate and the RO_2 destruction rate being higher than the production rate. Because differences are highest when the chemical system is dominated by the oxidation of myrcene and therefore the presence of MyO_2, reactions pathways of MyO_2 other than reactions with NO and HO_2 could be responsible for the imbalances.

As described in Section 2, MyO_2 isomerization reactions can become competitive at low NO mixing ratios like in these experiments (< 0.1 ppbv). Isomerization rates derived from SAR are applied (Section 2). Products of the 1,6 H-shift reactions in myrcene that correspond to similar reactions in isoprene could produce radicals like in the case of isoprene (Fig. 3). Products from the two additional isomerization reactions likely undergo fast ring-closure reactions on the di-methyl double bond and it is uncertain, if OH or HO_2 are directly produced. As an estimate for the potential impact of MyO_2 isomerization reactions on radical regeneration, production of one HOx radical from each isomerization reaction is assumed in the following. ~~As~~ Because the yield of OH and HO_2 from ~~MyO_2 isomerization~~ potential isomerization and decomposition reactions of MyO_2 is not known~~in this study~~, an upper limit ~~is used by assuming the yield of both~~ of one OH and one HO_2 ~~are unity~~radical for each isomerization reaction is applied. The results of this sensitivity analysis are shown in Fig. 11 and 12.

The bulk MyO_2 loss due to isomerization for the isomers that can rapidly interconvert (Fig. 2) are competitive with the reaction of MyO_2 with NO at mixing ratios of 0.5 to 1 ppbv making these reaction very competitive for conditions of the experiments. As shown in Fig. 12, the discrepancy between RO_2 radical production and destruction rates would be even over-compensated, if isomerization rates determined by SAR are applied. ~~The~~ Similar as for the RO_2 loss rate, potential production of OH and HO_2 ~~production rates also overwhelm their destruction rates, if the~~ from MyO_2 isomerization ~~yields equivalent~~

OH and HO_2 radicalsreactions would overcompensate the imbalances in their production and destruction rates. A sensitivity test shows that using a bulk isomerization reaction rate constant of $0.05\,s^{-1}$ instead of $0.02\,s^{-1}$ would be sufficient to balance the RO_2 production rate. This value is a factor 2 to 4 lower than bulk reaction rates calculated by SAR, but are still within the uncertainty of calculations.

Although this analysis shows the potential for high contributions of MyO_2 isomerization to the total loss rate of RO_2 for conditions that are typical for forested areas, the uncertainties are high concerning the isomerization rate constants and the yield of HO_x radicals. In addition, discrepancies of radical production and destruction rates within the range of 20 % of the total rate for single radical species can be observed even for well-known chemical systems as methane as shown in Section 5.2. This is likely due to uncertainties in the radical concentration measurements. Unaccounted systematic errors in the analysis may therefore also explain a significant fraction of the differences in radical production and destruction rates in the experiments with myrcene.

7 Summary and conclusions

The photooxidation of the monoterpene myrcene was investigated at atmospheric conditions in the simulation chamber SAPHIR at two different levels of NO. The chemical mechanism of the oxidation of myrcene by OH has not been investigated in detail so far. Based on the structural similarity with isoprene ($CH_2{=}CH{-}C(=CH_2)CH_2-$ moiety) and with 2-methyl-2-butene ($-CH_2{-}CH{=}C(CH_3)_2$ moiety) and structure-activity relationship (Peeters et al., 2007; Jenkin et al., 2019; Vereecken and Nozière, 2020) a chemical mechanism for the first oxidation step is proposed that includes rapid RO_2 interconversion by reversible oxygen addition and H-shift reactions of RO_2 like in isoprene. In addition to RO_2 isomerization reactions similar to that of isoprene derived RO_2, additional H-shift reactions are suggested by SAR, so that the overall impact of isomerization reactions in myrcene can be high, although only approximately half of the attack of OH to myrcene is on the isoprenyl part. Assuming that the interconversion of RO_2 is similar as in isoprene, bulk isomerization rate constants of $0.21\,s^{-1}$ and $0.097\,s^{-1}$ ($T = 298\,K$) for the 3 isomers resulting from the 3'-OH and 1-OH addition, respectively, are calculated using rate constants derived by SAR.

Experiments in the chamber allowed to determine the reaction rate constant of the reaction of myrcene with OH resulting in a value of $(2.3{\pm}0.3){\times}10^{-10}\,cm^3s^{-1}$, which is in good agreement with values reported in the literature within the uncertainties (Table 4). Product yields of acetone and formaldehyde calculated from measured time series of these species were found to be 0.45 ± 0.08 and 0.35 ± 0.08, respectively. Although these values well agree with studies by Reissell et al. (2002); Orlando et al. (2000) within the uncertainties, the formaldehyde yield is lower than expected for conditions of the experiment with NO mixing ratios of 200 pptv, if there are no RO_2 isomerization reactions. The lower yield would be consistent with competing RO_2 isomerization reactions that may not produce formaldehyde. From the analysis of nitrogen oxides in the chamber, the yield of organic nitrates in the myrcene oxidation could be determined to be 0.13 ± 0.03 in agreement with measurements by Lee et al. (2006) (0.10 ± 0.03). Both values are lower than typical values predicted by SAR (0.19, Jenkin et al. (2019) and found for monoterpene species which often range between 0.15 and 0.25. This may impact the formation of secondary organic

aerosol from the OH oxidation of myrcene compared to other monoterpene species. The applicability of the procedure for the determination of the organic nitrate yield was tested in photo-oxidation experiments with methane and α-pinene, both of which resulted in organic nitrate yields that well agree with expected values. This demonstrates that the method gives reliable results and can be applied in chamber experiments.

Radical production and destruction rates can be calculated using measured radical and trace gas concentrations. Total radical (RO_x) production and destruction rates are balanced in the experiments in this work, if the rate of the radical loss terminating the radical reaction chain due to recombination reactions of HO_2 and RO_2 was only 40 % of the loss expected from the reaction rate constant predicted by SAR or if this reaction would regenerate radicals instead of producing radical termination products (hydroperoxides). However, this conclusion has a high uncertainty of approximately a factor of 2 due to the uncertainty of radical production from myrcene ozonolysis.

Imbalances between radical production and destruction rates are observed for RO_2 radicals in the experiments with low NO concentrations, when MyO_2 isomerization reaction can become competitive with bi-molecular reactions. Bulk reaction rates constants around $0.05\,s^{-1}$ for MyO2 isomers which can quickly interconvert and which partly can isomerize, are a factor of 2 to 4 lower than reaction rates constants calculated by SAR, but values are consistent regarding the high uncertainty of the determination from experiments and the uncertainty of SAR calculations.

The analysis of radical concentrations measurements in field campaigns, where monoterpene emissions dominated the mix of organic compounds such as in Finland (Hens et al., 2014) and in the Rocky Mountains (Kim et al., 2013) showed that current chemical models cannot explain measured OH and HO_2 concentrations. The analysis of chamber experiments revealed that the OH oxidation of the most abundant monoterpene species α-pinene and β-pinene are not well understood (Kaminski et al., 2017; Rolletter et al., 2019). Experiments here show that also the reaction of OH with myrcene is complex due to the rapid RO_2 inter-conversion and H-shift RO_2 reactions. Therefore, short-comings in the description of the photo-oxidation of myrcene could contribute to explaining model-measurement discrepancies found in field campaigns.

Data availability. Data are available from the Eurochamp database (16 August 2012: https://doi.org/10.25326/5XRG-Y765, Fuchs et al. (2021a), 22 August 2012: https://doi.org/10.25326/9RAV-5450, Fuchs et al. (2021b), 17 July 2013: https://doi.org/10.25326/GP2K-R926, Fuchs et al. (2021c), 18 July 2013: https://doi.org/10.25326/JJ16-1S54, Fuchs et al. (2021d), 03 September 2019: https://doi.org/10.25326/PBBV-WF18, Fuchs et al. (2021e), 29 May 2020: https://doi.org/10.25326/MG6T-TW58, Fuchs et al. (2021f))

Author contributions. Z.T., L.H. and H.F. wrote the manuscript. M.K., R.W. and H.F. designed and led the experiments in the chamber. I.A. (organic compounds), B.B. (radiation), H.-P. D. (radicals), X.L. (HONO), S.N. (OH reactivity), F.R. (nitrogen oxides, ozone), R.T. (organic compunds), A.N. (radicals), C.C. (radicals) were responsible for measurements used in this work. All co-authors commented and discussed the manuscript and contributed thereby to the writing of the manuscript.

Competing interests. The authors declare that they have no conflict of interest.

Acknowledgements. This work was supported by the EU FP-7 program EUROCHAMP-2 (grant agreement no. 228335). This project has received funding from the European Research Council (ERC) under the European Union's Horizon 2020 research and innovation program (grant agreement no. 681529). S. Nehr and B. Bohn thank the Deutsche Forschungsgemeinschaft for funding (grant no. 1580/3-1). The authors thank Luc Vereecken for the discussion of the chemical mechanism.

References

Allen, H. M., Crounse, J. D., Bates, K. H., Teng, A. P., Krawiec-Thayer, M. P., Rivera-Rios, J. C., Keutsch, F. N., St. Clair, J. M., Hanisco, T. F., Møller, K. H., Kjaergaard, H. G., and Wennberg, P. O.: Kinetics and product yields of the OH initiated oxidation of hydroxymethyl hydroperoxide, J. Phys. Chem. A, 122, 6292–6302, https://doi.org/10.1021/acs.jpca.8b04577, 2018.

Aschmann, S. M., Atkinson, R., and Arey, J.: Products of reaction of OH radicals with α-pinene, J. Geophys. Res., 107, ACH 6–1–ACH 6–7, https://doi.org/10.1029/2001JD001098, 2002.

Atkinson, R.: Gase-phase tropospheric chemistry of volatile organic compounds: 1. alkanes and alkenes, J. Phys. Chem. Ref. Data, 26, 217–290, 1997.

Atkinson, R. and Arey, J.: Atmospheric degradation of volatile organic compounds, Chem. Rev., 103, 4605–4638, https://doi.org/10.1021/cr0206420, 2003.

Atkinson, R., Aschmann, S. M., and Pitts, J. N.: Rate constants for the gas-phase reactions of the OH radical with a series of monoterpenes at 294$\pm$1 K, Int. J. Chem. Kin., 18, 287–299, https://doi.org/10.1002/kin.550180303, 1986.

Atkinson, R., Baulch, D. L., Cox, R. A., Crowley, J. N., Hampson, R. F., Hynes, R. G., Jenkin, M. E., Rossi, M. J., and Troe, J.: Evaluated kinetic and photochemical data for atmospheric chemistry: Volume I - gas phase reactions of O_x, HO_x, NO_x and SO_x species, Atmos. Chem. Phys., 4, 1461-1738, https://doi.org/10.5194/acp-4-1461-2004, 2004.

Atkinson, R., Aschmann, S. M., Arey, J., and Shorees, B.: Formation of OH radicals in the gas phase reactions of O_3 with a series of terpenes, J. Geophys. Res., 97, 6065–6073, https://doi.org/10.1029/92jd00062, 1992.

Böge, O., Mutzel, A., Iinuma, Y., Yli-Pirilä, P., Kahnt, A., Joutsensaari, J., and Herrmann, H.: Gas-phase products and secondary organic aerosol formation from the ozonolysis and photooxidation of myrcene, Atmos. Environ., 79, 553–560, https://doi.org/10.1016/j.atmosenv.2013.07.034, 2013.

Bohn, B. and Zilken, H.: Model-aided radiometric determination of photolysis frequencies in a sunlit atmosphere simulation chamber, Atmos. Chem. Phys., 5, 191–206, https://doi.org/10.5194/acp-5-191-2005, 2005.

Bohn, B., Rohrer, F., Brauers, T., and Wahner, A.: Actinometric measurements of NO_2 photolysis frequencies in the atmosphere simulation chamber SAPHIR, Atmos. Chem. Phys., 5, 493–503, https://doi.org/10.5194/acp-5-493-2005, 2005.

Boyd, A. A., Flaud, P.-M., Daugey, N., and Lesclaux, R.: Rate constants for RO_2 + HO_2 reactions measured under a large excess of HO_2, J. Phys. Chem. A, 107, 818–821, https://doi.org/10.1021/jp026581r, 2003.

Browne, E. C., Wooldridge, P. J., Min, K. E., and Cohen, R. C.: On the role of monoterpene chemistry in the remote continental boundary layer, Atmos. Chem. Phys., 14, 1225–1238, https://doi.org/10.5194/acp-14-1225-2014, 2014.

Burkholder, J. B., Sander, S. P., Abbatt, J. P. D., Barker, J. R., Huie, R. E., Kolb, C. E., Kurylo, M. J., Orkin, V. L., Wilmouth, D. M., and Wine, P. H.: Chemical kinetics and photochemical data for use in atmospheric studies–evaluation number 19 (https://jpldataeval.jpl.nasa.gov/pdf/NASA-JPL%20Evaluationpanel for data evaluation technical report, 19-5, 2020.

Butkovskaya, N., Kukui, A., and Le Bras, G.: Pressure and temperature dependence of methyl nitrate formation in the CH_3O_2 + NO reaction, J. Phys. Chem. A, https://doi.org/10.1021/jp210710d, 2012.

Crounse, J. D., Knap, H. C., Ornso, K. B., Jorgensen, S., Paulot, F., Kjaergaard, H. G., and Wennberg, P. O.: On the atmospheric fate of methacrolein: 1. Peroxy radical isomerization following addition of OH and O_2, J. Phys. Chem. A, 116, 5756–5762, https://doi.org/10.1021/jp211560u, 2012.

Crounse, J. D., Nielsen, L. B., Jørgensen, S., Kjaergaard, H. G., and Wennberg, P. O.: Autoxidation of organic compounds in the atmosphere, J. Phys. Chem. Lett., 4, 3513–3520, https://doi.org/10.1021/jz4019207, 2013.

Deng, P., Wang, L., and Wang, L.: Mechanism of gas-phase ozonolysis of β-myrcene in the atmosphere, J. Phys. Chem. A, 122, 3013–3020, https://doi.org/10.1021/acs.jpca.8b00983, 2018.

Dorn, H.-P., Brandenburger, U., Brauers, T., and Hausmann, M.: A new in-situ laser long-path absorption instrument for the measurement of tropospheric OH radicals, J. Atmos. Sci., 52, 3373–3380, 1995.

Fuchs, H., Hofzumahaus, A., and Holland, F.: Measurement of tropospheric RO_2 and HO_2 radicals by a laser-induced fluorescence instrument, Rev. Sci. Instrum., 79, 084 104, https://doi.org/10.1063/1.2968712, 2008.

Fuchs, H., Bohn, B., Hofzumahaus, A., Holland, F., Lu, K. D., Nehr, S., Rohrer, F., and Wahner, A.: Detection of HO_2 by laser-induced fluorescence: calibration and interferences from RO_2 radicals, Atmos. Meas. Tech., 4, 1209–1255, https://doi.org/10.5194/amt-4-1209-2011, 2011.

Fuchs, H., Hofzumahaus, A., Rohrer, F., Bohn, B., Brauers, T., Dorn, H.-P., Häseler, R., Holland, F., Kaminski, M., Li, X., Lu, K., Nehr, S., Tillmann, R., Wegener, R., and Wahner, A.: Experimental evidence for efficient hydroxyl radical regeneration in isoprene oxidation, Nature Geosci., 6, 1023–1026, https://doi.org/10.1038/NGEO1964, 2013.

Fuchs, H., Acir, I. H., Bohn, B., Brauers, T., Dorn, H. P., Häseler, R., Hofzumahaus, A., Holland, F., Kaminski, M., Li, X., Lu, K., Lutz, A., Nehr, S., Rohrer, F., Tillmann, R., Wegener, R., and Wahner, A.: OH regeneration from methacrolein oxidation investigated in the atmosphere simulation chamber SAPHIR, Atmos. Chem. Phys., 14, 7895–7908, https://doi.org/10.5194/acp-14-7895-2014, 2014.

Fuchs, H., Tan, Z., Hofzumahaus, A., Broch, S., Dorn, H.-P., Holland, F., Kuenstler, C., Gomm, S., Rohrer, F., Schrade, S., Tillmann, R., and Wahner, A.: Investigation of potential interferences in the detection of atmospheric ROx radicals by laser-induced fluorescence under dark conditions, Atmos. Meas. Tech., 9, 1431-1447, https://doi.org/10.5194/amt-9-1431-2016, 2016.

Fuchs, H., Tan, Z., Lu, K., Bohn, B., Broch, S., Brown, S. S., Dong, H., Gomm, S., Häseler, R., He, L., Hofzumahaus, A., Holland, F., Li, X., Liu, Y., Lu, S., Min, K. E., Rohrer, F., Shao, M., Wang, B., Wang, M., Wu, Y., Zeng, L., Zhang, Y., Wahner, A., and Zhang, Y.: OH reactivity at a rural site (Wangdu) in the North China Plain: contributions from OH reactants and experimental OH budget, Atmos. Chem. Phys., 17, 645–661, https://doi.org/10.5194/acp-17-645-2017, 2017.

Fuchs, H., Albrecht, S., Acir, I. H., Bohn, B., Breitenlechner, M., Dorn, H. P., Gkatzelis, G. I., Hofzumahaus, A., Holland, F., Kaminski, M., Keutsch, F. N., Novelli, A., Reimer, D., Rohrer, F., Tillmann, R., Vereecken, L., Wegener, R., Zaytsev, A., Kiendler-Scharr, A., and Wahner, A.: Investigation of the oxidation of methyl vinyl ketone (MVK) by OH radicals in the atmospheric simulation chamber SAPHIR, Atmos. Chem. Phys., 2018, 8001–8016, https://doi.org/10.5194/acp-18-8001-2018, 2018.

Fuchs, H., Kaminski, M., Acir, I.-H., Bohn, B., Dorn, H.-P., Nehr, S., Rohrer, F., Tillmann, R., Wegener, R., and Li, X.: Atmospheric simulation chamber study: myrcene + OH - Gas-phase oxidation - product study [Data set]. AERIS. https://doi.org/10.25326/5XRG-Y765, 2021a.

Fuchs, H., Kaminski, M., Acir, I.-H., Bohn, B., Dorn, H.-P., Nehr, S., Rohrer, F., Tillmann, R., Wegener, R., and Li, X.: Atmospheric simulation chamber study: myrcene + OH - Gas-phase oxidation - product study [Data set]. AERIS. https://doi.org/10.25326/9RAV-54505, 2021b.

Fuchs, H., Kaminski, M., Acir, I.-H., Bohn, B., Dorn, H.-P., Nehr, S., Rohrer, F., Tillmann, R., Wegener, R., and Li, X.: Atmospheric simulation chamber study: myrcene + OH - Gas-phase oxidation - product study [Data set]. AERIS. https://doi.org/10.25326/GP2K-R926, 2021c.

Fuchs, H., Kaminski, M., Acir, I.-H., Bohn, B., Dorn, H.-P., Nehr, S., Rohrer, F., Tillmann, R., Wegener, R., and Li, X.: Atmospheric simulation chamber study: myrcene + OH - Gas-phase oxidation - product study [Data set]. AERIS. https://doi.org/10.25326/JJ16-1S54, 2021d.

Fuchs, H., Bohn, B., Rohrer, F., Tillmann, R., Cho, C., and Novelli, A.: Atmospheric simulation chamber study: alpha-pinene + OH - Gas-phase oxidation - product study [Data set]. AERIS. https://doi.org/10.25326/JJ16-1S54, 2021e.

Fuchs, H., Rohrer, F., Bohn, B., Cho, C., and Novelli, A.: Atmospheric simulation chamber study: myrcene + OH - Reference experiment [Data set]. AERIS. https://doi.org/10.25326/MG6T-TW58, 2021f.

Galloway, M. M., Huisman, A. J., Yee, L. D., Chan, A. W. H., Loza, C. L., Seinfeld, J. H., and Keutsch, F. N.: Yields of oxidized volatile organic compounds during the OH radical initiated oxidation of isoprene, methyl vinyl ketone, and methacrolein under high-NO_X conditions, Atmos. Chem. Phys., 11, 10 779–10 790, https://doi.org/10.5194/acp-11-10779-2011, 2011.

Glowania, M., Rohrer, F., Dorn, H. P., Hofzumahaus, A., Holland, F., Kiendler-Scharr, A., Wahner, A., and Fuchs, H.: Comparison of formaldehyde measurements by Hantzsch, CRDS and DOAS in the SAPHIR chamber, Atmos. Meas. Tech., 14 4239-4253, https://doi.org/10.5194/amt-14-4239-2021, 2021.

Grimsrud, E. P., Westberg, H. H., and Rasmussen, R. A.: Atmospheric reactivity of monoterpene hydrocarbons, NO, photooxidation and ozonolysis, Int. J. Chem. Kin., 7:Suppl. 1, 183–195, 1975.

Guenther, A. B., Jiang, X., Heald, C. L., Sakulyanontvittaya, T., Duhl, T., Emmons, L. K., and Wang, X.: The model of emissions of gases and aerosols from nature version 2.1 (MEGAN2.1): an extended and updated framework for modeling biogenic emissions, Geosci. Model Dev., 5, 1471–1492, https://doi.org/10.5194/gmd-5-1471-2012, 2012.

Helmig, D., Daly, R. W., Milford, J., and Guenther, A.: Seasonal trends of biogenic terpene emissions, Chemosphere, 93, 35–46, https://doi.org/10.1016/j.chemosphere.2013.04.058, 2013.

Hens, K., Novelli, A., Martinez, M., Auld, J., Axinte, R., Bohn, B., Fischer, H., Keronen, P., Kubistin, D., Nölscher, A. C., Oswald, R., Paasonen, P., Petäjä, T., Regelin, E., Sander, R., Sinha, V., Sipilä, M., Taraborrelli, D., Tatum Ernest, C., Williams, J., Lelieveld, J., and Harder, H.: Observation and modelling of HO_X radicals in a boreal forest, Atmos. Chem. Phys., 14, 8723–8747, https://doi.org/10.5194/acp-14-8723-2014, 2014.

Hites, R. A. and Turner, A. M.: Rate constants for the gas-phase β-myrcene + OH and isoprene + OH reactions as a function of temperature, Int. J. Chem. Kin., 41, 407–413, https://doi.org/10.1002/kin.20413, 2009.

Hofzumahaus, A., Rohrer, F., Lu, K., Bohn, B., Brauers, T., Chang, C.-C., Fuchs, H., Holland, F., Kita, K., Kondo, Y., Li, X., Lou, S., Shao, M., Zeng, L., Wahner, A., and Zhang, Y.: Amplified trace gas removal in the troposphere, Science, 324, 1702–1704, https://doi.org/10.1126/science.1164566, 2009.

IUPAC: IUPAC Task Group on Atmospheric Chemical Kinetic Data Evaluation, s, p. last access 23 November 2020, 2020.

Jenkin, M. E., Valorso, R., Aumont, B., Rickard, A. R., and Wallington, T. J.: Estimation of rate coefficients and branching ratios for gas-phase reactions of OH with aliphatic organic compounds for use in automated mechanism construction, Atmospheric Chemistry and Physics, 18, 9297-9328, https://doi.org/10.5194/acp-18-9297-2018, 2018.

Jenkin, M. E., Valorso, R., Aumont, B., and Rickard, A. R.: Estimation of rate coefficients and branching ratios for reactions of organic peroxy radicals for use in automated mechanism construction, Atmos. Chem. Phys., 19, 7691–7717, https://doi.org/10.5194/acp-19-7691-2019, 2019.

Kaminski, M., Fuchs, H., Acir, I. H., Bohn, B., Brauers, T., Dorn, H. P., Häseler, R., Hofzumahaus, A., Li, X., Lutz, A., Nehr, S., Rohrer, F., Tillmann, R., Vereecken, L., Wegener, R., and Wahner, A.: Investigation of the β-pinene photooxidation by OH in the atmosphere simulation chamber SAPHIR, Atmos. Chem. Phys., 17, 6631–6650, https://doi.org/10.5194/acp-17-6631-2017, 2017.

Kim, D., Stevens, P. S., and Hites, R. A.: Rate constants for the gas-phase reactions of OH and O_3 with β-ocimene, β-myrcene, and α- and β-farnesene as a function of temperature, J. Chem. Phys. A, 115, 500-506, https://doi.org/10.1021/jp111173s, 2011.

Kim, S., Wolfe, G. M., Mauldin, L., Cantrell, C., Guenther, A., Karl, T., Turnipseed, A., Greenberg, J., Hall, S. R., Ullmann, K., Apel, E., Hornbrook, R., Kajii, Y., Nakashima, Y., Keutsch, F. N., DiGangi, J. P., Henry, S. B., Kaser, L., Schnitzhofer, R., Graus, M., Hansel, A., Zheng, W., and Flocke, F. F.: Evaluation of HO_x sources and cycling using measurement-constrained model calculations in a 2-methyl-3-butene-2-ol (MBO) and monoterpene (MT) dominated ecosystem, Atmos. Chem. Phys., 13, 2031–2044, https://doi.org/10.5194/acp-13-2031-2013, 2013.

Kostiainen, R.: Volatile organic compounds in the indoor air of normal and sick houses, Atmos. Environ., 29, 693–702, https://doi.org/10.1016/1352-2310(94)00309-9, 1995.

Lee, A., Goldstein, A. H., Kroll, J. H., Ng, N. L., Varutbangkul, V., Flagan, R. C., and Seinfeld, J. H.: Gas-phase products and secondary aerosol yields from the photooxidation of 16 different terpenes, J. Geophys. Res., 111, n/a–n/a, https://doi.org/10.1029/2006JD007050, 2006.

Lelieveld, J., Butler, T. M., Crowley, J. N., Dillon, T. J., Fischer, H., Ganzeveld, L., Harder, H., Lawrence, M. G., Martinez, M., Taraborrelli, D., and Williams, J.: Atmospheric oxidation capacity sustained by a tropical forest, Nature, 452, 737–740, https://doi.org/10.1038/nature06870, 2008.

Li, X., Rohrer, F., Hofzumahaus, A., Brauers, T., Häseler, R., Bohn, B., Broch, S., Fuchs, H., Gomm, S., Holland, F., Jäger, J., Kaiser, J., Keutsch, F. N., Lohse, I., Lu, K., Tillmann, R., Wegener, R., Wolfe, G. M., Mentel, T. F., Kiendler-Scharr, A., and Wahner, A.: Missing gas-phase source of HONO inferred from Zeppelin measurements in the troposphere, Science, 344, 292–296, https://doi.org/10.1126/science.1248999, 2014.

Liu, Y. J., Herdlinger-Blatt, I., McKinney, K. A., and Martin, S. T.: Production of methyl vinyl ketone and methacrolein via the hydroperoxyl pathway of isoprene oxidation, Atmos. Chem. Phys. Discuss., 12, 33 323–33 358, https://doi.org/10.5194/acpd-12-33323-2012, 2012.

Lockhart, J., Blitz, M., Heard, D., Seakins, P., and Shannon, R.: Kinetic study of the OH + glyoxal reaction: Experimental evidence and quantification of direct OH recycling, J. Phys. Chem. A, 117, 11 027–11 037, https://doi.org/10.1021/jp4076806, 2013.

Lou, S., Holland, F., Rohrer, F., Lu, K., Bohn, B., Brauers, T., Chang, C. C., Fuchs, H., Häseler, R., Kita, K., Kondo, Y., Li, X., Shao, M., Zeng, L., Wahner, A., Zhang, Y., Wang, W., and Hofzumahaus, A.: Atmospheric OH reactivities in the Pearl River Delta - China in summer 2006: measurement and model results, Atmos. Chem. Phys., 10, 11 243–11 260, https://doi.org/10.5194/acp-10-11243-2010, 2010.

Novelli, A., Kaminski, M., Rolletter, M., Acir, I. H., Bohn, B., Dorn, H. P., Li, X., Lutz, A., Nehr, S., Rohrer, F., Tillmann, R., Wegener, R., Holland, F., Hofzumahaus, A., Kiendler-Scharr, A., Wahner, A., and Fuchs, H.: Evaluation of OH and HO_2 concentrations and their budgets during photooxidation of 2-methyl-3-butene-2-ol (MBO) in the atmospheric simulation chamber SAPHIR, Atmos. Chem. Phys., 18, 11 409–11 422, https://doi.org/10.5194/acp-18-11409-2018, 2018.

Novelli, A., Vereecken, L., Bohn, B., Dorn, H. P., Gkatzelis, G. I., Hofzumahaus, A., Holland, F., Reimer, D., Rohrer, F., Rosanka, S., Taraborrelli, D., Tillmann, R., Wegener, R., Yu, Z., Kiendler-Scharr, A., Wahner, A., and Fuchs, H.: Importance of isomerization reactions for OH radical regeneration from the photo-oxidation of isoprene investigated in the atmospheric simulation chamber SAPHIR, Atmos. Chem. Phys., 20, 3333–3355, https://doi.org/10.5194/acp-20-3333-2020, 2020.

Noziére, B., Barnes, I., and Becker, K.-H.: Product study and mechanisms of the reactions of α-pinene and of pinonaldehyde with OH radicals, J. Geophys. Res., 104, 23 645–23 656, https://doi.org/10.1029/1999JD900778, 1999.

Orlando, J. J., Nozière, B., Tyndall, G. S., Orzechowska, G. E., Grazyna, E., Paulson, S. E., and Rudich Y.: Product studies of the OH- and ozone-initiated oxidation of some monoterpenes, J.Geophys. Res., 105, 11561–11572, https://doi.org/10.1029/200JD900005, 2000.

Paulot, F., Crounse, J. D., Kjaergaard, H. G., Kroll, J. H., Seinfeld, J. H., and Wennberg, P. O.: Isoprene photooxidation: new insights into the production of acids and organic nitrates, Atmos. Chem. Phys., 9, 1479–1501, https://doi.org/10.5194/acp-9-1479-2009, 2009.

Peeters, J., Boullart, W., Pultau, V., Vandenberk, S., and Vereecken, L.: Structure–activity relationship for the addition of OH to (poly)alkenes: site-specific and total rate constants, J. Phys. Chem. A, 111, 1618–1631, https://doi.org/10.1021/jp066973o, 2007.

Peeters, J., Nguyen, T. L., and Vereecken, L.: HO_X radical regeneration in the oxidation of isoprene, Phys. Chem. Chem. Phys., 11, 5935–5939, https://doi.org/10.1039/b908511d, 2009.

Peeters, J., Müller, J.-F., Stavrakou, T., and Nguyen, V. S.: Hydroxyl radical recycling in isoprene oxidation driven by hydrogen bonding and hydrogen tunneling: The upgraded LIM1 mechanism, J. Phys. Chem. A, 118, 8625–8643, https://doi.org/10.1021/jp5033146, 2014.

Praske, E., Otkjær, R. V., Crounse, J. D., Hethcox, J. C., Stoltz, B. M., Kjaergaard, H. G., and Wennberg, P. O.: Atmospheric autoxidation is increasingly important in urban and suburban North America, Proc. Nat. Acadamy. Sci., 115, 64–69, https://doi.org/10.1073/pnas.1715540115, 2018.

Praske, E., Otkjaer, R. V., Crounse, J. D., Hethcox, J. C., Stoltz, B. M., Kjaergaard, H. G., and Wennberg, P. O.: Intramolecular hydrogen shift chemistry of hydroperoxy-substituted peroxy radicals, J. Phys. Chem. A, 123, 590–600, https://doi.org/10.1021/acs.jpca.8b09745, 2019.

Reissell, A., Aschmann, S. M., Atkinson, R., and Arey, J.: Products of the OH radical- and O_3-initiated reactions of myrcene and ocimene, J. Geophys. Res., 107, ACH 3–1–ACH 3–6, https://doi.org/10.1029/2001JD001234, 2002.

Rindelaub, J. D., McAvey, K. M., and Shepson, P. B.: The photochemical production of organic nitrates from α-pinene and loss via acid-dependent particle phase hydrolysis, Atmos. Environ., 100, 193–201, https://doi.org/10.1016/j.atmosenv.2014.11.010, 2015.

Rohrer, F., Bohn, B., Brauers, T., Brüning, D., Johnen, F.-J., Wahner, A., and Kleffmann, J.: Characterisation of the photolytic HONO-source in the atmosphere simulation chamber SAPHIR, Atmos. Chem. Phys., 5, 2189–2201, https://doi.org/10.5194/acp-5-2189-2005, 2005.

Rolletter, M., Kaminski, M., Acir, I. H., Bohn, B., Dorn, H. P., Li, X., Lutz, A., Nehr, S., Rohrer, F., Tillmann, R., Wegener, R., Hofzumahaus, A., Kiendler-Scharr, A., Wahner, A., and Fuchs, H.: Investigation of the α-pinene photooxidation by OH in the atmospheric simulation chamber SAPHIR, Atmos. Chem. Phys., 19, 11 635–11 649, https://doi.org/10.5194/acp-19-11635-2019, 2019.

Rolletter, M., Blocquet, M., Kaminski, M., Bohn, B., Dorn, H. P., Hofzumahaus, A., Holland, F., Li, X., Rohrer, F., Tillmann, R., Wegener, R., Kiendler-Scharr, A., Wahner, A., and Fuchs, H.: Photooxidation of pinonaldehyde at ambient conditions investigated in the atmospheric simulation chamber SAPHIR, Atmos. Chem. Phys., 20, 13 701–13 719, https://doi.org/10.5194/acp-20-13701-2020, 2020.

Schlosser, E., Brauers, T., Dorn, H.-P., Fuchs, H., Häseler, R., Hofzumahaus, A., Holland, F., Wahner, A., Kanaya, Y., Kajii, Y., Miyamoto, K., Nishida, S., Watanabe, K., Yoshino, A., Kubistin, D., Martinez, M., Rudolf, M., Harder, H., Berresheim, H., Elste, T., Plass-Dülmer, C., Stange, G., and Schurath, U.: Technical Note: Formal blind intercomparison of OH measurements: results from the international campaign HOxComp, Atmos. Chem. Phys., 9, 7923–7948, https://doi.org/10.5194/acp-9-7923-2009, 2009.

Scholtens, K. W., Messer, B. M., Cappa, C. D., and Elrod, M. J.: Kinetics of the CH_3O_2+NO reaction: Temperature dependence of the overall rate constant and improved upper limit for the CH_3ONO_2 branching channel, J. Geophys. Res., 100, 18 811–18 816, https://doi.org/10.1021/jp990469k, 1995.

Schwantes, R. H., Emmons, L. K., Orlando, J. J., Barth, M. C., Tyndall, G. S., Hall, S. R., Ullmann, K., St. Clair, J. M., Blake, D. R., Wisthaler, A., and Bui, T. P. V.: Comprehensive isoprene and terpene gas-phase chemistry improves simulated surface ozone in the southeastern US, Atmos. Chem. Phys., 20, 3739–3776, https://doi.org/10.5194/acp-20-3739-2020, 2020.

Sindelarova, K., Granier, C., Bouarar, I., Guenther, A., Tilmes, S., Stavrakou, T., Müller, J. F., Kuhn, U., Stefani, P., and Knorr, W.: Global data set of biogenic VOC emissions calculated by the MEGAN model over the last 30 years, Atmos. Chem. Phys., 14, 9317–9341, https://doi.org/10.5194/acp-14-9317-2014, 2014.

Tan, Z., Fuchs, H., Lu, K. D., Hofzumahaus, A., Bohn, B., Broch, S., Dong, H. B., Gomm, S., Haseler, R., He, L. Y., Holland, F., Li, X., Liu, Y., Lu, S. H., Rohrer, F., Shao, M., Wang, B. L., Wang, M., Wu, Y. S., Zeng, L. M., Zhang, Y. S., Wahner, A., and Zhang, Y. H.: Radical chemistry at a rural site (Wangdu) in the North China Plain: observation and model calculations of OH, HO_2, and RO_2 radicals, Atmos. Chem. Phys., 17, 663-690, https://doi.org/10.5194/acp-17-663-2017, 2017.

Tan, Z., Lu, K., Hofzumahaus, A., Fuchs, H., Bohn, B., Holland, F., Liu, Y., Rohrer, F., Shao, M., Sun, K., Wu, Y., Zeng, L., Zhang, Y., Zou, Q., Kiendler-Scharr, A., Wahner, A., and Zhang, Y.: Experimental budgets of OH, HO_2, and RO_2 radicals and implications for ozone formation in the Pearl River Delta in China 2014, Atmos. Chem. Phys., 19, 7129–7150, https://doi.org/10.5194/acp-19-7129-2019, 2019.

Tan, Z., Hofzumahaus, A., Lu, K., Brown, S. S., Holland, F., Huey, L. G., Kiendler-Scharr, A., Li, X., Liu, X., Ma, N., Min, K.-E., Rohrer, F., Shao, M., Wahner, A., Wang, Y., Wiedensohler, A., Wu, Y., Wu, Z., Zeng, L., Zhang, Y., and Fuchs, H.: No evidence for a significant impact of heterogeneous chemistry on radical concentrations in the North China Plain in summer 2014, Environ Sci. Technol., 54, 5973–5979, https://doi.org/10.1021/acs.est.0c00525, 2020.

Teng, A. P., Crounse, J. D., and Wennberg, P. O.: Isoprene peroxy radical dynamics, J. Am. Chem. Soc., 139, 5367–5377, https://doi.org/10.1021/jacs.6b12838, 2017.

Vereecken, L. and Peeters, J.: Decompositon of substituted alkoxy radicals - Part I: a generalized structure-activy relationship for reaction barrier heights, Phys. Chem. Chem. Phys., 11, 9062–9074, https://doi.org/10.1039/B909712K, 2009.

Vereecken, L. and Peeters, J.: A structure-activy relationship for the rate coefficients of H-migration in substituted alkoxy radicals, Phys. Chem. Chem. Phys., 12, 120608–12620, https://doi.org/10.1039/C0CP00387E, 2010.

Vereecken, L. and Nozière, B.: H migration in peroxy radicals under atmospheric conditions, Atmos. Chem. Phys., 20, 7429–7458, https://doi.org/10.5194/acp-20-7429-2020, 2020.

Vereecken, L., Carlsson, P. T. M., Novelli, A., Bernard, F., Brown, S. S., Cho, C., Crowley, J. N., Fuchs, H., Mellouki, W., Reimer, D., Shenolikar, J., Tillmann, R., Zhou, L., Kiendler-Scharr, A. and Wahner, A.: Theoretical and experimental study of peroxy and alkoxy radicals in the NO_3-initiated oxidation of isoprene, Phys. Chem. Chem. Phys., 23, 5496–5515, https://doi.org/10.1039/D0CP06267G, 2021a.

Vereecken, L.: personal communication, 2021b.

Wegener, R., Brauers, T., Koppmann, R., Bares, S. R., Rohrer, F., Tillmann, R., Wahner, A., Hansel, A., and Wisthaler, A.: Simulation chamber investigation of the reactions of ozone with short-chained alkenes, J. Geophys. Res., 112, D13 301, https://doi.org/10.1029/2006JD007531, 2007.

Wennberg, P. O., Bates, K. H., Crounse, J. D., Dodson, L. G., McVay, R. C., Mertens, L. A., Nguyen, T. B., Praske, E., Schwantes, R. H., Smarte, M. D., St Clair, J. M., Teng, A. P., Zhang, X., and Seinfeld, J. H.: Gas-Phase Reactions of Isoprene and Its Major Oxidation Products, Chem. Rev., 118, 3337-3390, https://doi.org/10.1021/acs.chemrev.7b00439, 2018.

Whalley, L. K., Edwards, P. M., Furneaux, K. L., Goddard, A., Ingham, T., Evans, M. J., Stone, D., Hopkins, J. R., Jones, C. E., Karunaharan, A., Lee, J. D., Lewis, A. C., Monks, P. S., Moller, S. J., and Heard, D. E.: Quantifying the magnitude of a missing hydroxyl radical source in a tropical rainforest, Atmos. Chem. Phys., 11, 7223–7233, https://doi.org/10.5194/acp-11-7223-2011, 2011.

Xu, L., Guo, H., Boyd, C. M., Klein, M., Bougiatioti, A., Cerully, K. M., Hite, J. R., Isaacman-VanWertz, G., Kreisberg, N. M., Knote, C., Olson, K., Koss, A., Goldstein, A. H., Hering, S. V., de Gouw, J., Baumann, K., Lee, S.-H., Nenes, A., Weber, R. J., and Ng, N. L.: Effects of anthropogenic emissions on aerosol formation from isoprene and monoterpenes in the southeastern United States, Proc. Nat. Acadamy. Sci., 112, 37–42, https://doi.org/10.1073/pnas.1417609112, 2015.

Zhang, H. F., Yee, L. D., Lee, B. H., Curtis, M. P., Worton, D. R., Isaacman-VanWertz, G., Offenberg, J. H., Lewandowski, M., Kleindienst, T. E., Beaver, M. R., Holder, A. L., Lonneman, W. A., Docherty, K. S., Jaoui, M., Pye, H. O. T., Hu, W. W., Day, D. A., Campuzano-Jost, P., Jimenez, J. L., Guo, H. Y., Weber, R. J., de Gouw, J., Koss, A. R., Edgerton, E. S., Brune, W., Mohr, C., Lopez-Hilfiker, F. D., Lutz, A., Kreisberg, N. M., Spielman, S. R., Hering, S. V., Wilson, K. R., Thornton, J. A., and Goldstein, A. H.: Monoterpenes are the largest source of summertime organic aerosol in the southeastern United States, Proc. Nat. Acad. Sci., 115, 2038–2043, https://doi.org/10.1073/pnas.1717513115, 2018.

Table 1. Experimental conditions for the oxidation experiments. Concentrations are given for the conditions in the SAPHIR chamber at the time of the first VOC injection.

date	type of VOC	VOC / ppbv	NO / ppbv	O_3 / ppbv	T / K	RH / %
16 August 2012	myrcene	2.3	0.2	< 20	305	30.7
22 August 2012	myrcene	2.3	0.2	< 15	310	10.1
17 July 2013	myrcene	0.8	0.06	40	305	57.7
18 July 2013	myrcene	0.8	0.09	40	308	32.0
29 May 2020	methane	140000	0.23	60 - 120	303	22.1
03 September 2019	α-pinene	8.5	0.1	8	296	24.0

Table 2. Instrumentation for radical and trace gas detection in the experiments.

measured quantity	measurement technique	time resolution	precision ($1\,\sigma$)	accuracy ($1\,\sigma$)
OH	differential optical absorption spectroscopy	205 s	0.6×10^6 cm^{-3}	6.5 %
OH	laser-induced fluoresence (LIF)	47 s	0.4×10^6 cm^{-3}	13 %
HO_2, RO_2	laser-induced fluoresence (LIF)	47 s	1.5×10^7 cm^{-3}	16 %
MyO_2				50 %
k_{OH}	laser photolysis + LIF	180 s	0.3 s^{-1}	10 %, $\pm$0.7 s^{-1}
myrcene, α-pinene	proton-transfer-reaction mass-spectrometry	40 s	15 pptv	7 %
myrcene, aceton	gas-chromatography	30 min	100 pptv	6 %
CH_4	cavity ring-down spectroscopy	60 s	1 ppbv	3 ppbv
CO	cavity ring-down spectroscopy	60 s	25 ppbv	1 ppbv
NO	chemiluminescence	180 s	~~4~~13 pptv	5 %
NO_2	photolytic converter + chemiluminescence	180 s	~~2~~30 pptv	~~5~~7 %
HONO	long-path absorption photometry	300 s	7 pptv	20 %
O_3	UV-absorption	10 s	1 ppbv	5 %
HCHO	differential optical absorption spectroscopy	100 s	20 %	10 %
HCHO	Hantzsch method (Aerolaser)	90 s	100 pptv	10 %
photolysis freq.	actinic flux spectroradiometry	60 s	10 %	10 %

Table 3. Chemical reactions considered in the radical budget analysis of OH, HO_2 and RO_2. Some reactions are only applicable in the experiment with either methane, α-pinene or myrcene, in which specific RO_2 radicals, CH_3O_2, MyO_2 or APO_2 are formed. RO_2+RO_2 reactions are not listed, because they do not significantly contribute to the loss of radicals for conditions of experiments here.

	Reaction	k(T=298 K, P=1 atm)	uncertainty[a]	reference
radical initiation reactions				
R1	HONO+hν (<400 nm) $\rightarrow$ OH+NO	j_{HONO}	22 %	measured
R2	O_3+hν (<340 nm) $\rightarrow$ $O(^1D)$+O_2	$j_{\mathrm{O(^1D)}}$	11 %	measured
	$O(^1D)$+H_2O $\rightarrow$ OH+OH	2.1×10^{-10} cm^{3}s^{-1}		IUPAC (2020)
	$O(^1D)$+M $\rightarrow$ $O(^3P)$+M	3.3×10^{-11} cm^{3}s^{-1}		IUPAC (2020)
R3	HCHO+hν (<335 nm)+$2O_2$ $\rightarrow$ $2HO_2$+CO	j_{HCHO}	11 %	measured
R4	O_3+myrc $\rightarrow$ 0.71 OH+0.71 RO_2	3.9×10^{-16} cm^{3}s^{-1}	22 %	Deng et al. (2018); Kim et al. (2011)
radical propagation reactions				
R5	HO_2+NO $\rightarrow$ OH+ NO_2	8.5×10^{-12} cm^{3}s^{-1}	27 %	IUPAC (2020)
R6	HO_2+O_3 $\rightarrow$ OH+ 2 O_2	2.0×10^{-15} cm^{3}s^{-1}	20 %	IUPAC (2020)
R7	OH+VOC+O_2 $\rightarrow$ RO_2			
	RO_2 = CH_3O_2	6.4×10^{-15} cm^{3}s^{-1}	17 %	IUPAC (2020)
	RO_2 = MyO_2	2.3×10^{-10} cm^{3}s^{-1}	25 %	this work
R8	OH+HCHO+O_2 $\rightarrow$ HO_2+CO +H_2O	8.4×10^{-12} cm^{3}s^{-1}	25 %	IUPAC (2020)
R9	OH+CO+O_2 $\rightarrow$ HO_2 + CO_2	2.3×10^{-13} cm^{3}s^{-1}	17 %	IUPAC (2020)
R10	OH+O_3 $\rightarrow$ HO_2+O_2	7.3×10^{-14} cm^{3}s^{-1}	17 %	IUPAC (2020)
R11	RO_2+NO $\rightarrow$ HO_2+NO_2+R′CHO [c]			
	RO_2 = CH_3O_2	7.7×10^{-12} cm^{3}s^{-1}	27 %	IUPAC (2020)
	RO_2 = MyO_2	$0.87\times9.1\times10^{-12}$ cm^{3}s^{-1}	55 %	IUPAC (2020)[b]
radical termination reactions				
R12	OH+NO_2 $\rightarrow$ HNO_3	1.2×10^{-11} cm^{3}s^{-1}	28 %	IUPAC (2020)
R13	OH+NO $\rightarrow$ HONO	9.8×10^{-12} cm^{3}s^{-1}	28 %	IUPAC (2020)
R14	RO_2+NO $\rightarrow$ $RONO_2$			
	RO_2 = CH_3O_2	≈0	-	IUPAC (2020)
	RO_2 = APO_2	$0.18\times9.1\times10^{-12}$ cm^{3}s^{-1}	27 %	IUPAC (2020)[b]
	RO_2 = MyO_2	$0.13\times9.1\times10^{-12}$ cm^{3}s^{-1}	55 %	IUPAC (2020)[b]
R15	$RO_{2,\mathrm{myrc}}$+HO_2 $\rightarrow$ ROOH +O_2	9.1×10^{-12} cm^{3}s^{-1}	25 %	this work
R16	HO_2+HO_2 + H_2O $\rightarrow$ H_2O_2 +O_2 + H_2O	4.0×10^{-13} cm^{3}s^{-1} [d]	25 %	IUPAC (2020)

[a] Uncertainty measurements (Table 2) and kinetic rate constants (10 % for reactions of inorganic and methyl peroxy radicals and 15 % for other)

[b] Reaction rate constant: IUPAC (2020); the branching ratio of 0.87 is taken from this work

[c] The dominant reaction of alkoxy radical is to form HO_2 which is not rate limiting for RO_2 to HO_2 conversion

[d] Effective reaction rate constant for 1 % H_2O mixing ratio

Table 4. Rate constants of the myrcene + OH reaction at 298 K.

$k\,\mathrm{cm^3 s^{-1}}$	method	reference
$(2.1 \pm 0.2) \times 10^{-10}$	relative rate technique	Atkinson et al. (1986)
$(3.4^{+1.5}_{-1.0}) \times 10^{-10}$	relative rate technique	Hites and Turner (2009)
1.8×10^{-10}	structure-activity relationship	Peeters et al. (2007)
1.9×10^{-10}	structure-activity relationship	Jenkin et al. (2018)
$(2.3 \pm 0.3) \times 10^{-10}$	direct measurement	this work

Table 5. Products yields from the reaction of myrcene with OH.

product	yield	temperature / K	reference
formaldehyde	0.30 ± 0.06	n.a.	Orlando et al. (2000)
	0.74 ± 0.08	294	Lee et al. (2006)
	0.35 ± 0.08	293-330	this work
acetone	0.36 ± 0.05	n.a.	Orlando et al. (2000)
	0.45 ± 0.06	296 ± 2	Reissell et al. (2002)
	0.22 ± 0.02	294	Lee et al. (2006)
	0.45 ± 0.08	293-330	this work
organic nitrate	0.10 ± 0.03	294	Lee et al. (2006)
	0.13 ± 0.03	293-330	this work

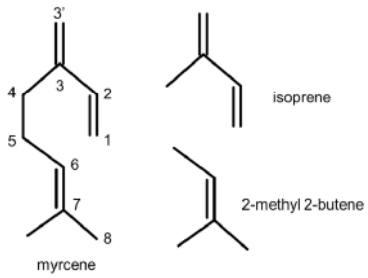

Figure 1. Chemical structures of myrcene, isoprene and 2-methyl 2-butene.

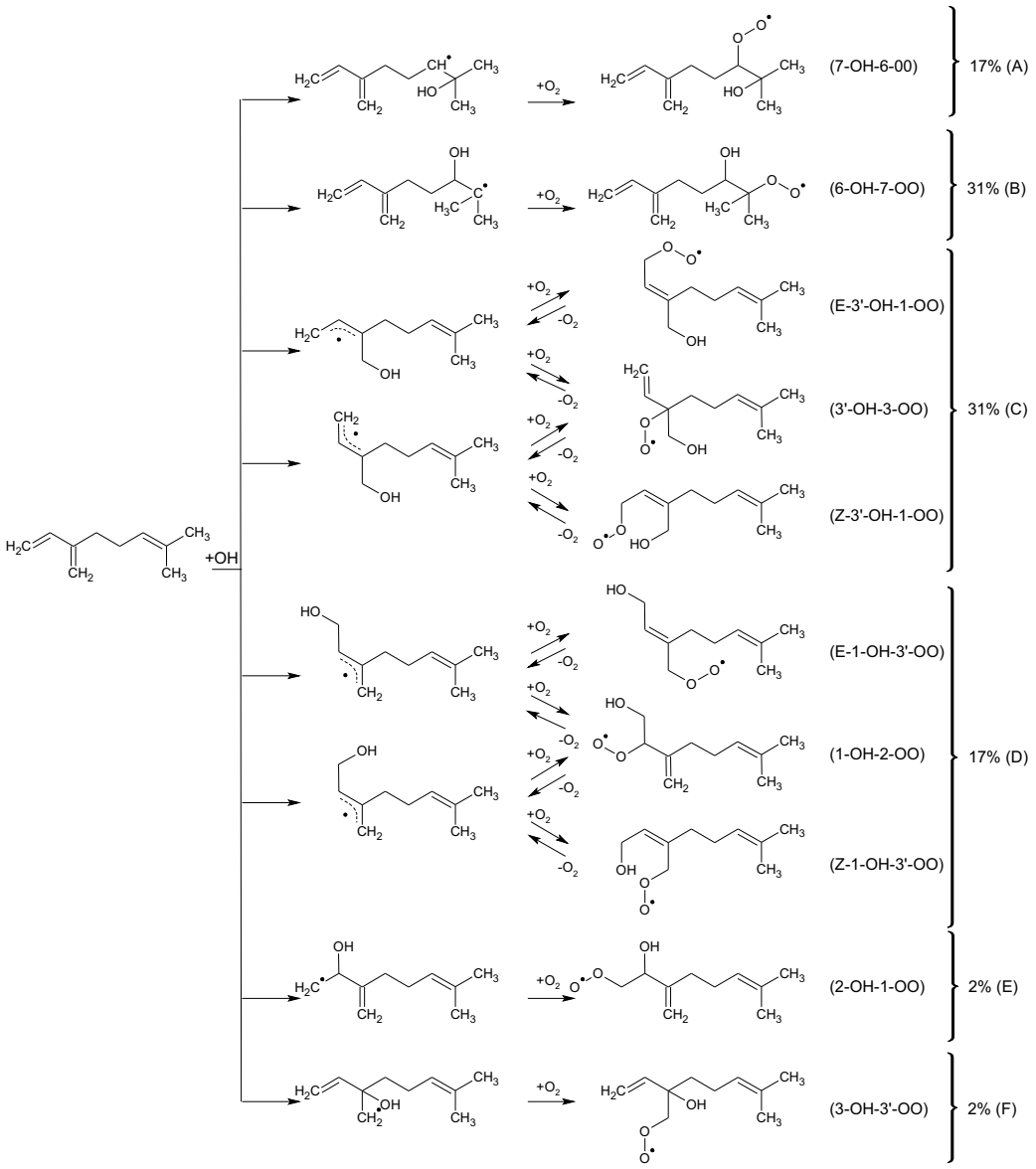

Figure 2. Peroxy radicals formed in the addition of OH to the double bonds in myrcence. $\mathrm{MyO_2}$ formed from the OH addition to the isoprenyl part of myrcene leads to the formation of $\mathrm{MyO_2}$ species that are expected to rapidly interconvert by oxygen abstraction and elimination like in isoprene (Peeters et al., 2014). Assuming reaction rate constants for oxygen abstraction and elimination like in isoprene, $3'-\mathrm{OH}-3-\mathrm{OO}$ and $1-\mathrm{OH}-2-\mathrm{OO}$ are expected to have the highest yields among the $\mathrm{MyO_2}$ species that can interconvert. $\mathrm{MyO_2}$ yields are predicted using SAR by Peeters et al. (2007).

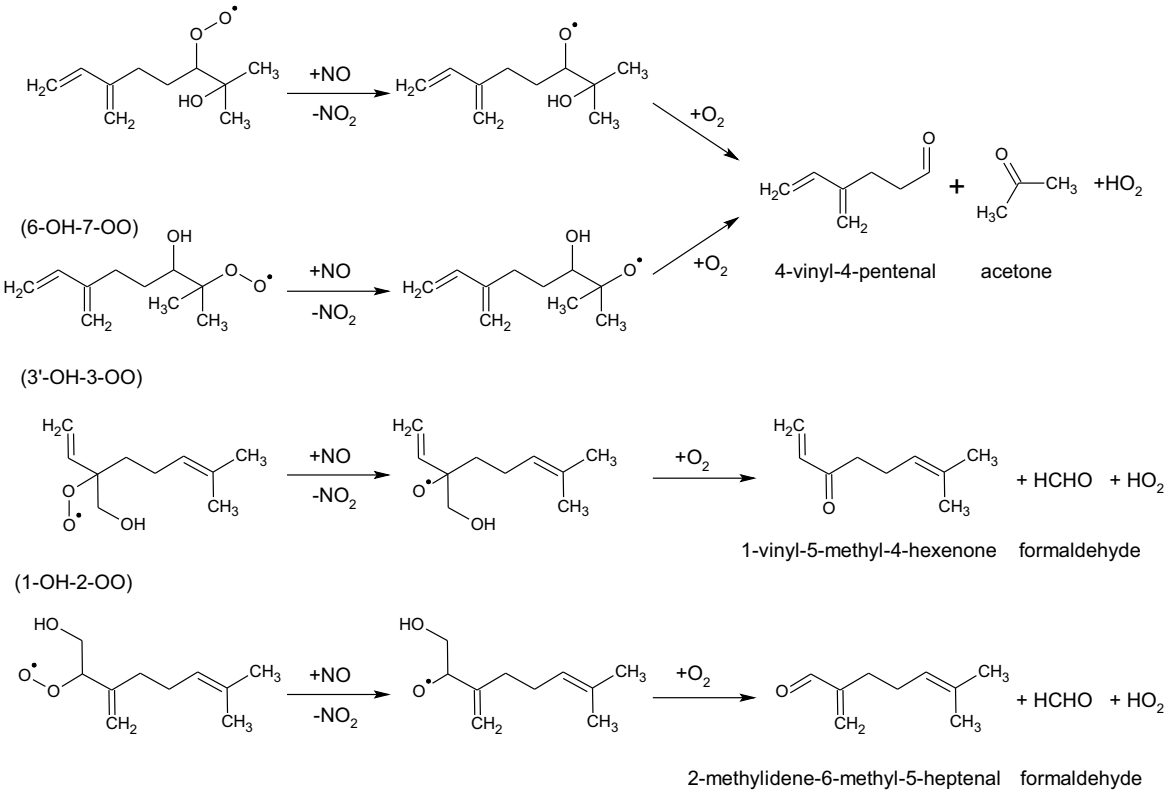

Figure 3. Reactions of the four most abundant myrcene hydroxy peroxy radicals with NO forming HO_2 and carbonyl compounds.

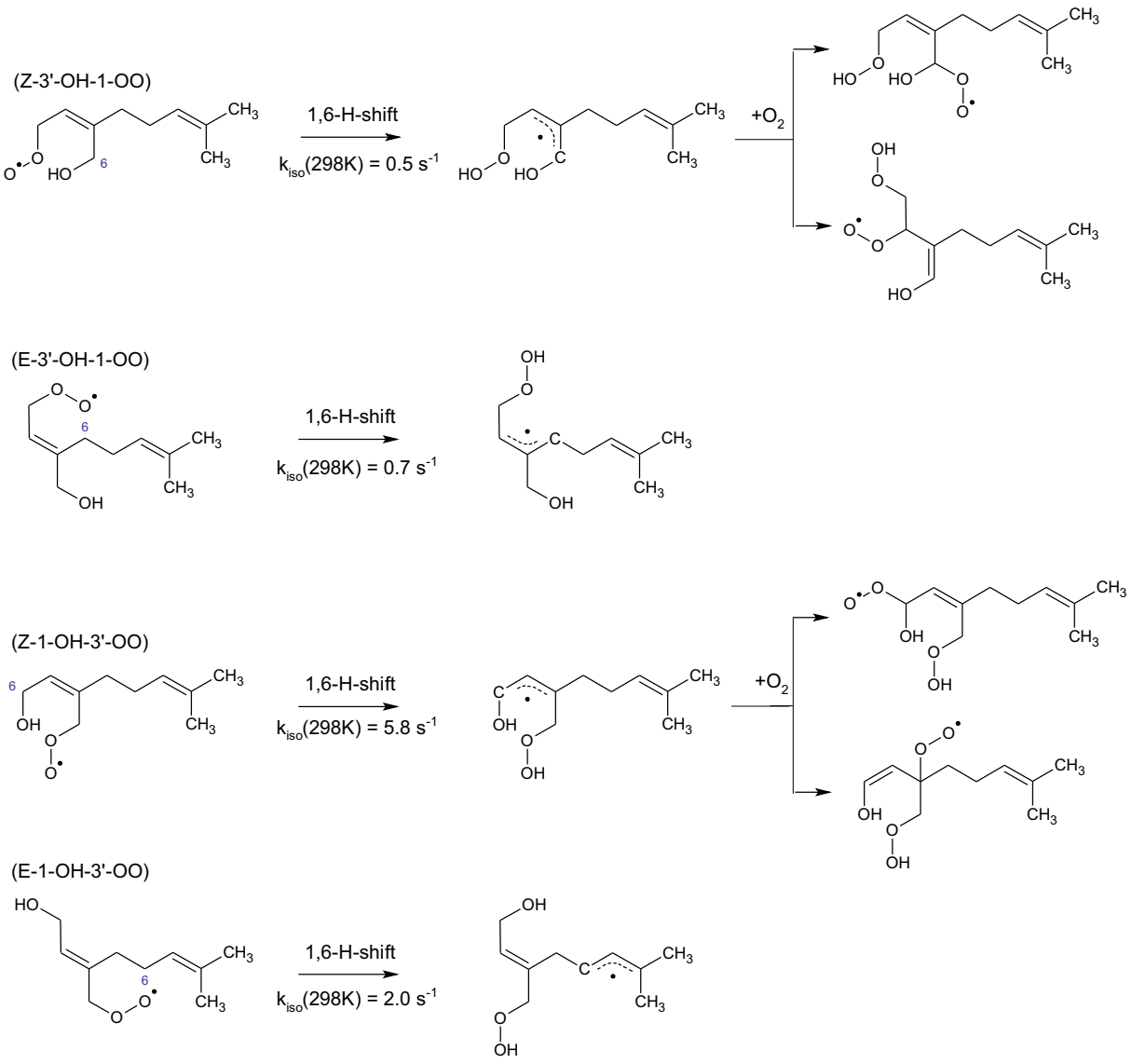

Figure 4. Fast H-shift reactions of myrcene peroxy radicals. Rate constants apply to 298 K. They are adopted for the $\mathrm{Z{-}3'{-}OH{-}1{-}OO}$ and $\mathrm{Z{-}1{-}OH{-}3'{-}OO}$ isomers from the corresponding 1,6-H-shift reactions of isoprene peroxy radicals (Peeters et al., 2014). Similar subsequent chemistry like for isoprene leads to the formation of peroxy radicals, some of which rapidly decompose. The isomerization reaction rate constants for the $\mathrm{E{-}3'{-}OH{-}1{-}OO}$ and $\mathrm{E{-}1{-}OH{-}3'{-}OO}$ peroxy radicals are calculated using SAR by Vereecken and Nozière (2020). Subsequent chemistry of products from these reactions likely undergo fast ring-closure reactions on the dimethyl double bond (not shown here).

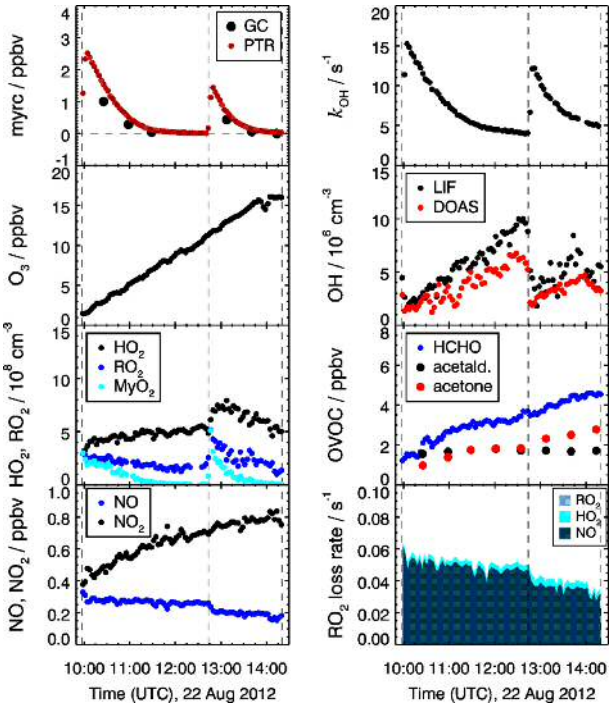

Figure 5. Trace gas and radical concentrations in the chamber experiment investigating the OH oxidation of myrcene (myrc) at NO mixing ratios between 200 and 300 pptv on 22 August 2012. Peroxy radicals from the reaction of OH with myrcene (MyO_2) and total organic peroxy radical (RO_2=MyO_2+$RO_{2,other}$) concentrations are calculated from observed radical concentrations as explained in Section 3.4. In the lowest right panel, the loss rates of total RO_2 with respect to their reaction with NO and radical recombination reactions are shown.

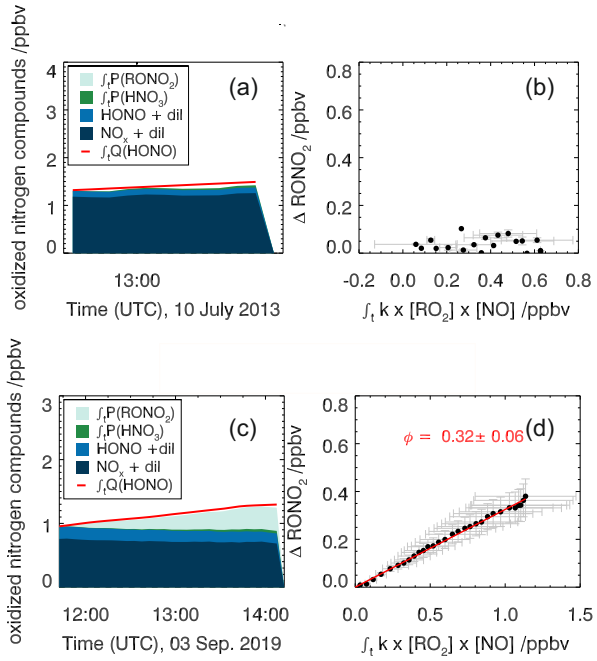

Figure 6. Time series of nitrogen oxide species in the experiments with methane (10 July 2013, (a)) and α-pinene (03 September 2019, (c)). The red lines in panels (a) and (c) are time integrated HONO emissions calculated as described in the text. NO_x and HONO concentrations were measured, the time integrated NO_2 loss by HNO_3 formation from the reaction of NO_2 with OH and the time integrated NO_2 loss by $RONO_2$ formation from the reaction of RO_2 with NO were calculated as described in the text. The alkyl nitrate yield (Φ_{RONO2}) is determined from the regression analysis (red line, panel (d)) using Equation 8. Errors are derived from error propagation of measurements.

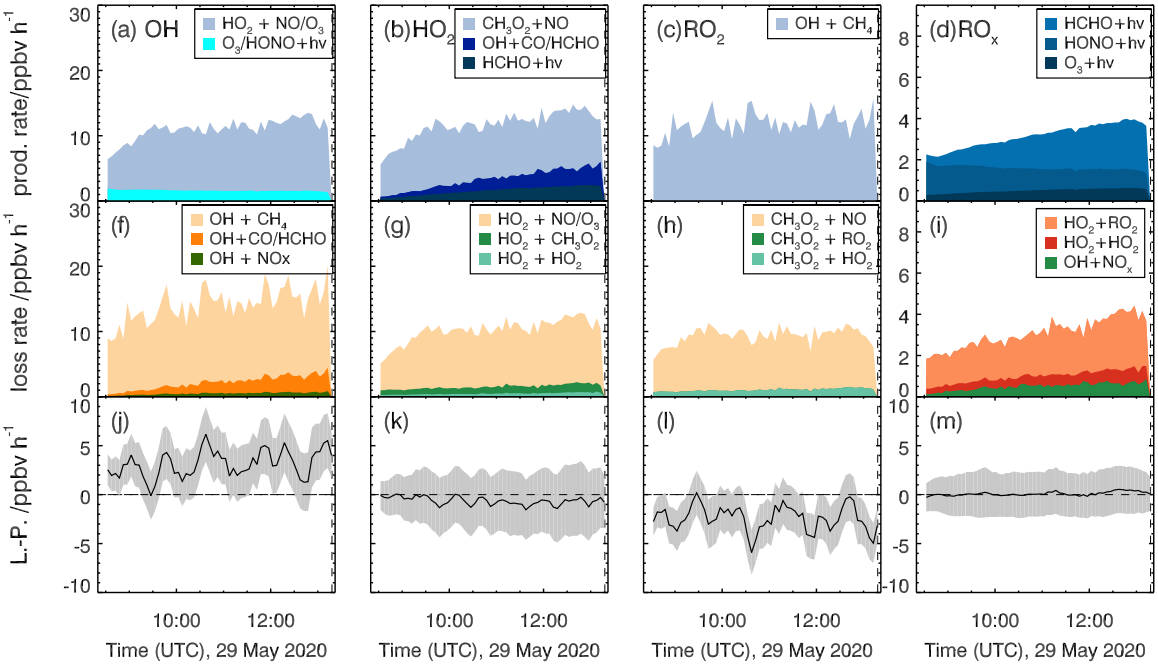

Figure 7. Calculated production and destruction rates of reactions involving radicals for the reference experiment with methane (29 May 2020). Production rates for OH, HO_2, RO_2 and total RO_x are shown in panels (a), (b), (c) and (d), respectively and loss rates for OH, HO_2, RO_2 and total RO_x are shown in panels (f), (g), (h) and (i). Lower panels (j) – (m) show the differences between loss and production rates ($L - P$) with the associated accuracy (grey areas).

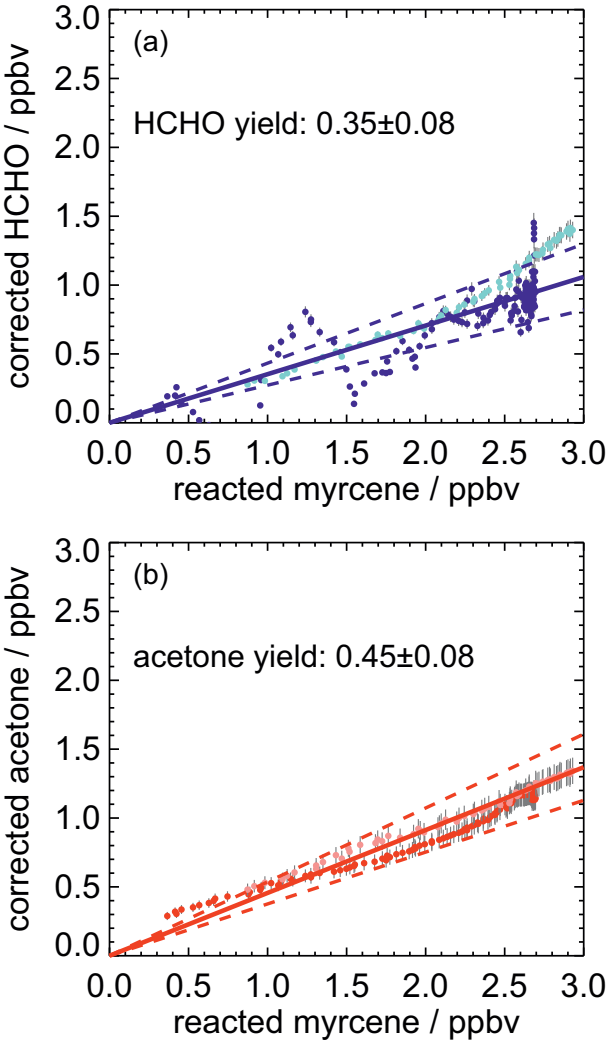

Figure 8. *(Revised)*Corrected product concentrations versus the myrcene that reacted away with OH for two experiments with medium NO (light colors: 16 August 2012, dark colors: 22 August 2012). Corrections are applied to account for formation of product species not connected to the oxidation of myrcene (chamber sources) and loss processes (reaction with OH, photolysis). The slopes of linear fits (solid lines) give the product yields of HCHO and acetone from the myrcene reaction with OH. The uncertainties of the yield calculations are indicated by dashed lines.

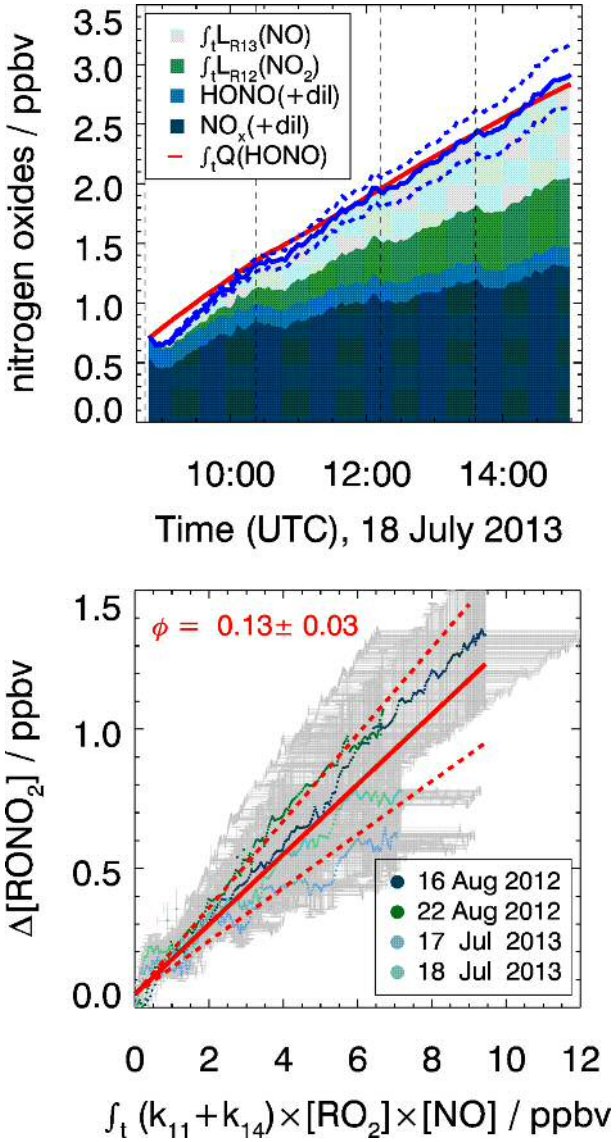

Figure 9. Determination of the organic nitrate yield from the production of nitrogen oxide species ($Q(\mathrm{HONO})$) in the chamber experiment. Upper panel: Example of cumulated reactive nitrogen oxide mixing ratios over the course of the experiment on 18 July 2013. The blue line denotes the total production of nitrogen oxides including organic nitrate applying a nitrate yield (Φ_{RONO2}) of 0.13. Dashed lines show the error of the total nitrogen oxide calculation. Lower panel: Scatter plot of integrated turnover rate of the reaction of $\mathrm{RO_2}$ with NO versus the unaccounted nitrogen oxide mixing ratios (ΔNOy, Equation 8). Results from all four experiments are included. The organic nitrate yield is determined by the slope of regression analysis (red line, $R^2 = 0.92$). Error bars denotes experimental uncertainty derived from the accuracy of the measurements (Table 2) and dashed red lines the resulting uncertainty in the slope of the regression analysis.

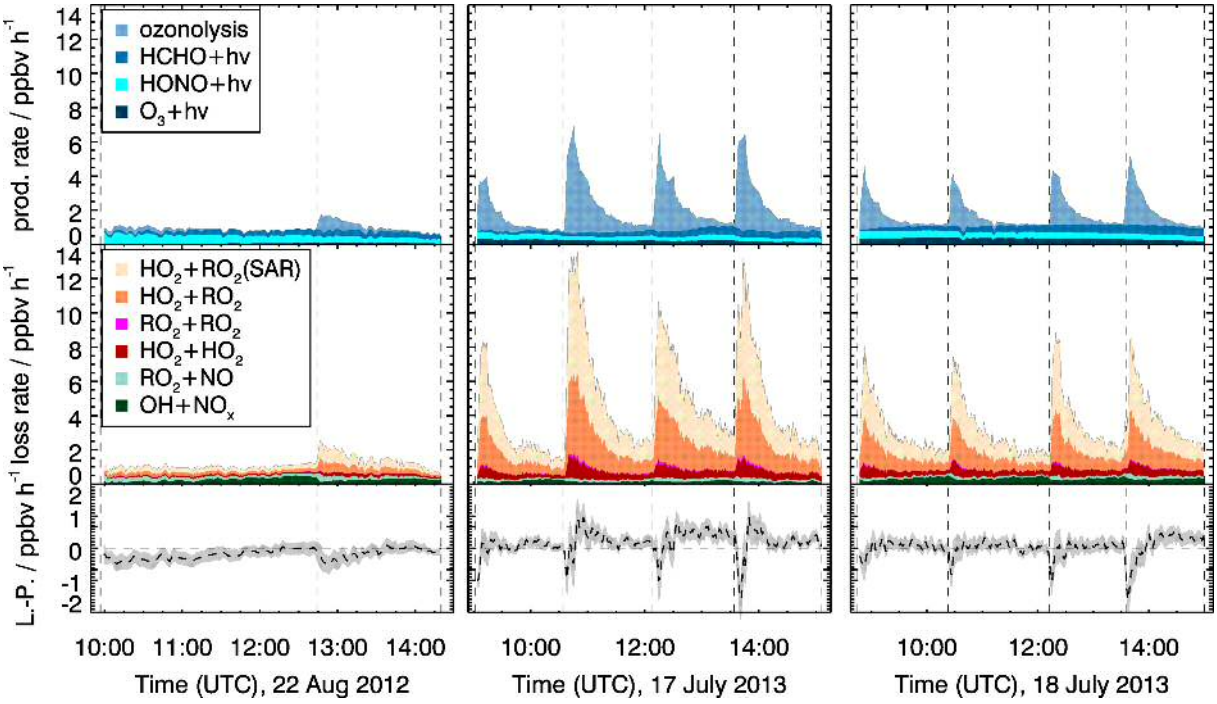

Figure 10. ***(Revised)*** RO_x primary production, P, (upper panels), termination L (middle panels) rates and their difference (lower panels). ~~Grey areas in the lower panels give the uncertainty of the difference between radical destruction and production ($L - P$).~~ The rate constant of the reaction of MyO_2 with HO_2 was adjusted, to minimize the difference between radical production and destruction (see text for more explanation). The HO_2+RO_2(SAR) shows the additional radical loss if the unadjusted reaction rate constant is applied. In the bottom row, the ~~cyan~~ lines show the ~~results~~ difference between radical destruction and production ($L - P$) with ~~non-adjusted reaction~~ adjusted rate constant of the reaction of MyO_2 with HO_2. Grey areas in the lower panels give the uncertainty of $L - P$.

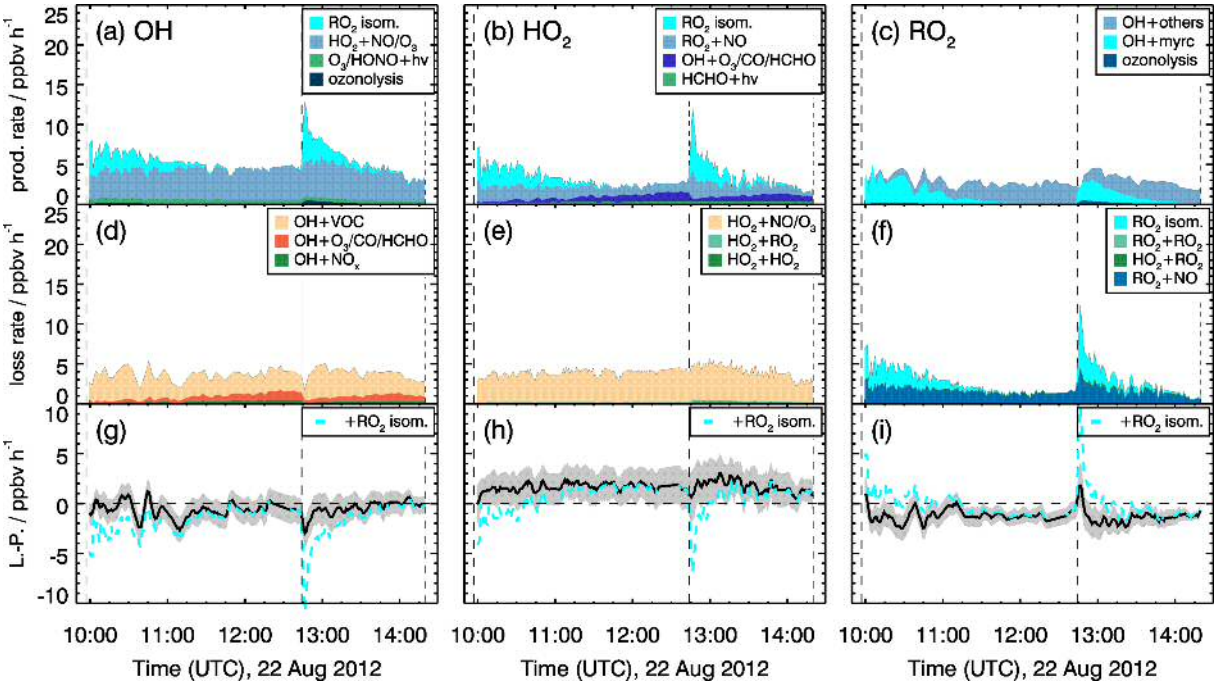

Figure 11. *(Revised)*Rates of radical conversion reactions and imbalances between production and destruction rates ($L - P$) for the experiment with medium NO mixing ratios (0.15 to 0.30 ppbv) on 22 August 2012. Grey areas in the lower panels give the uncertainty of the calculation ($L - P$). In the ~~lowest right panel~~bottom row, the black and cyan lines denote ~~loss rates~~ radical budget without and with considering MyO_2 isomerization reactions. ~~In panels (g) and (h), the maximum influence is shown by assuming unity yield~~ Upper limits for yields of OH and HO_2 radicals from MyO_2 isomerization reactions of one are assumed in the calculations of their production rates.

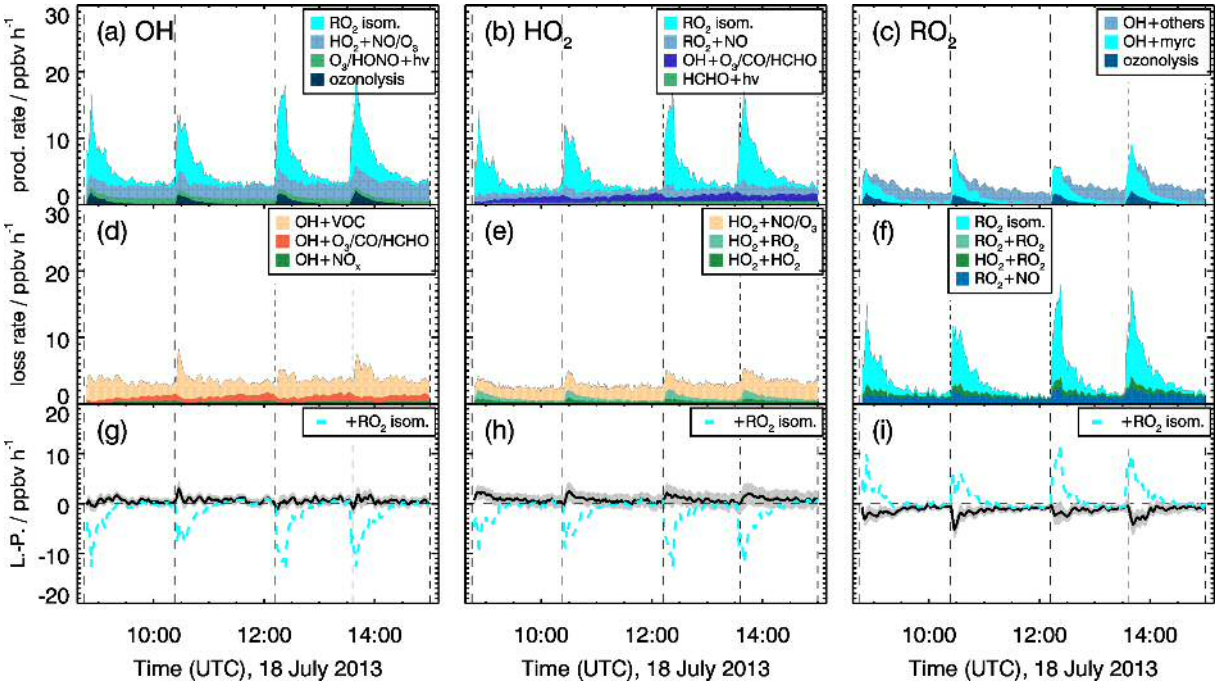

Figure 12. ***(Revised)***Rates of radical production and destruction reactions for OH, HO_2 and RO_2 for experiments at low NO mixing ratio (<0.11 ppbv) on 18 July 2013. Grey areas in the lower panels give the uncertainty of $L - P$. In the ~~lowest right panel~~bottom row, the black and cyan lines denote radical budget without and with considering MyO_2 isomerization reactions. ~~In panels (g) and (h), the maximum influence is shown by assuming unity yield~~ Upper limits for yields of OH and HO_2 radicals from MyO_2 isomerization reactions of one are assumed in the calculations of their production rates.

Supporting Information to "Atmospheric photo-oxidation of myrcene: OH reaction rate constant, gas phase oxidation products and radical budgets"

Zhaofeng Tan[1], Luisa Hantschke[1], Martin Kaminski[1,a], Ismail-Hakki Acir[1,b], Birger Bohn[1], Changmin Cho[1], Hans-Peter Dorn[1], Xin Li[1,c], Anna Lutz[2], Anna Novelli[1], Sascha Nehr[1,d], Franz Rohrer[1], Ralf Tillmann[1], Robert Wegener[1], Andreas Hofzumahaus[1], Astrid Kiendler-Scharr[1], Andreas Wahner[1], and Hendrik Fuchs[1]

[1]Institute of Energy and Climate Research, IEK-8: Troposphere, Forschungszentrum Jülich GmbH, Jülich, Germany
[2]Department of Chemistry and Molecular Biology, University of Gothenburg, Gothenburg, Sweden
[a]now at: Federal Office of Consumer Protection and Food Safety, Department 5: Method Standardisation, Reference Laboratories, Resistance to Antibiotics, Berlin, Germany
[b]now at: Institute of Nutrition and Food Sciences, Food Science, University of Bonn, Bonn, Germany
[c]now at: State Key Joint Laboratory of Environmental Simulation and Pollution Control, College of Environmental Sciences and Engineering, Peking University, Beijing, China
[d]now at: European University of Applied Sciences, Brühl, Germany

Correspondence: Hendrik Fuchs (h.fuchs@fz-juelich.de)

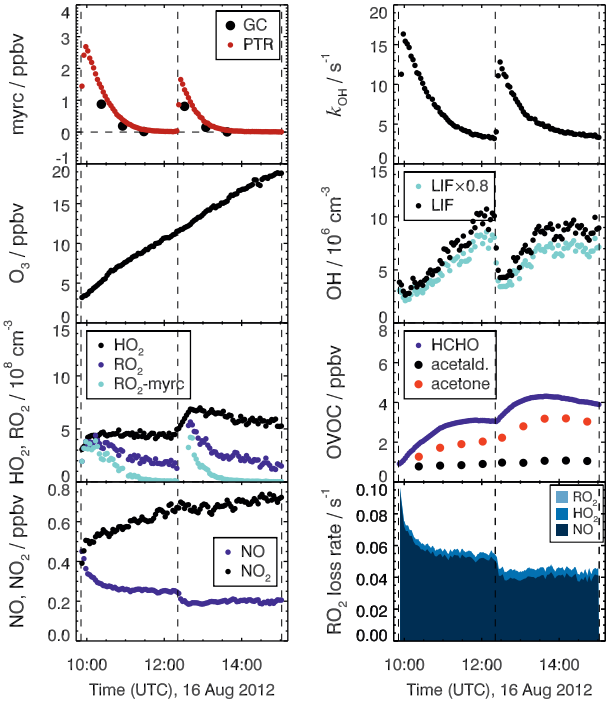

Figure 1. Overview of time series of trace gas and radical concentrations in the chamber experiment investigating the OH oxidation of myrcene (myrc) for medium NO mixing ratios on 16 August 2012. Total organic peroxy radical (RO_2) concentrations and RO_2 from the reaction of OH with myrcene were calculated from observations as explained in Section 2.4. In additions to trace gases, the loss rates of RO_2 with respect to their reaction with NO and radical recombination reactions are shown. OH measurements by LIF were scaled by a factor of 0.8 because the comparison between OH and DOAS hints to an calibration error of LIF measurements.

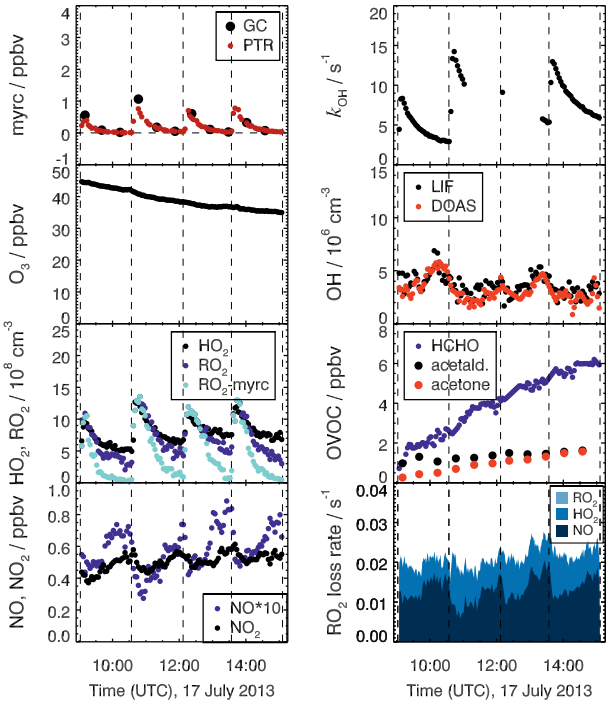

Figure 2. Same as Fig. S1, but for the experiment with myrcene at low NO conditions on 17 July 2013.

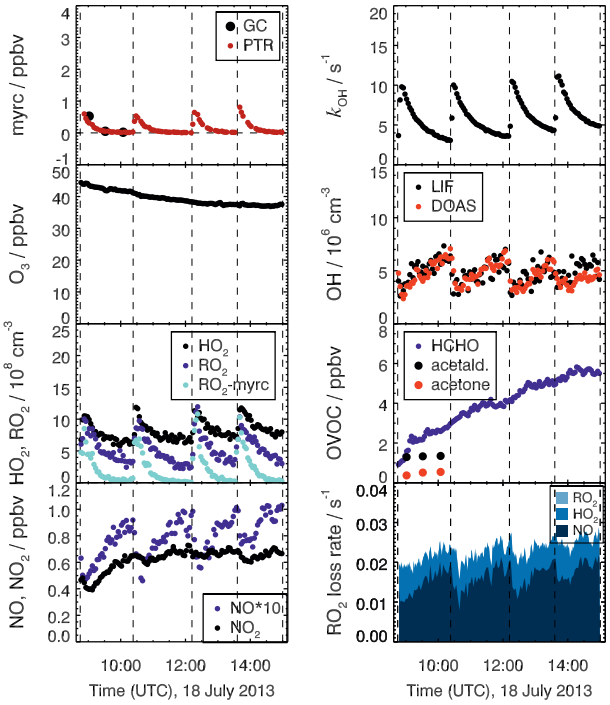

Figure 3. Same as Fig. S1, but for the experiment with myrcene at low NO conditions on 18 July 2013.

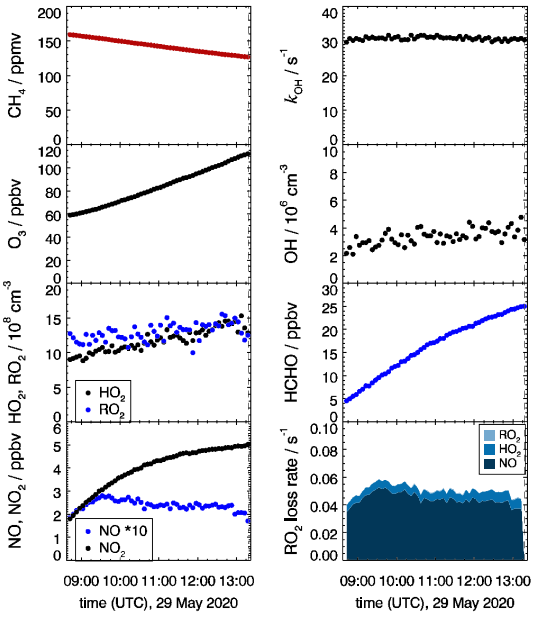

Figure 4. Same as Fig. S1, but for the experiment with methane on 29 May 2020.

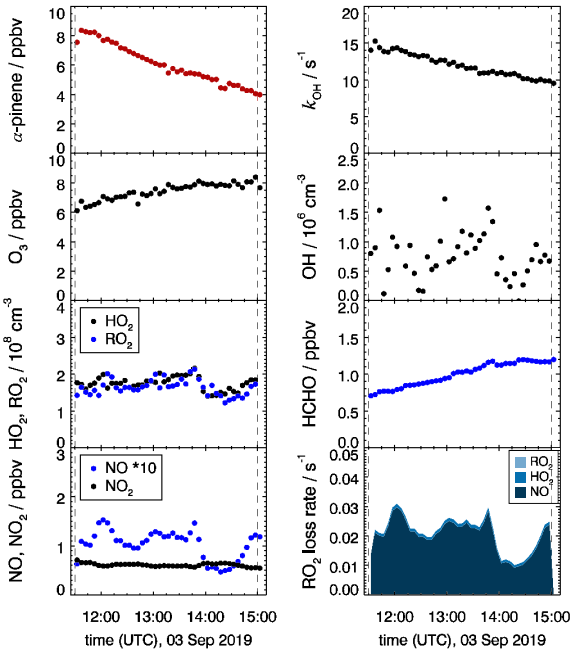

Figure 5. Same as Fig. S1, but for the experiment with α-pinene on 03 September 2019.

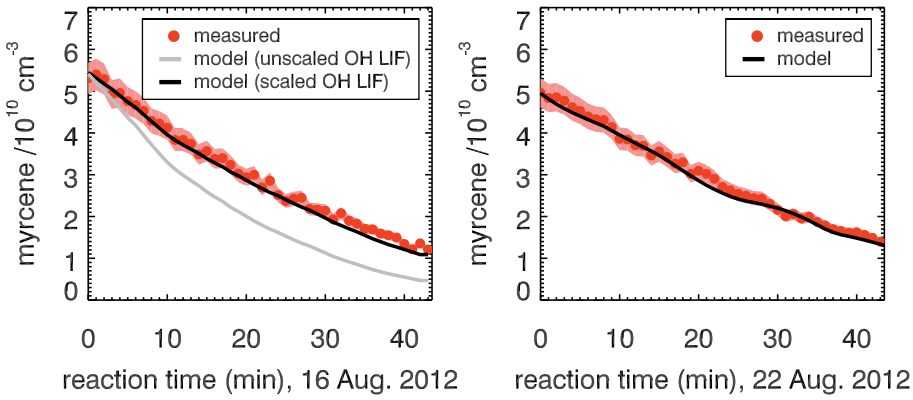

Figure 6. Comparison of the measured time series of myrcene concentrations with results from model calculations on 22 August 2012 (left panel) and 16 August 2012 (right panel). The model is constrained to measured temperature, pressure, ozone and OH concentrations and the rate constant of the reaction of myrcene with OH was optimized resulting in a value of $2.1 \times 10^{-10} molecules\,\mathrm{cm}^{-3}\mathrm{s}^{-1}$. OH was measured on 22 August by DOAS and LIF and only by LIF on 16 August. The comparison of OH and DOAS measurements on 22 August revealed that LIF measurements need to be scaled by a factor of 0.8, most likely due to a calibration error. Therefore, also measurements on 16 August are scaled by a factor of 0.8. Model results demonstrates that the scaling of the OH measurements is also required to describe the measured behaviour of myrcene in this experiment.

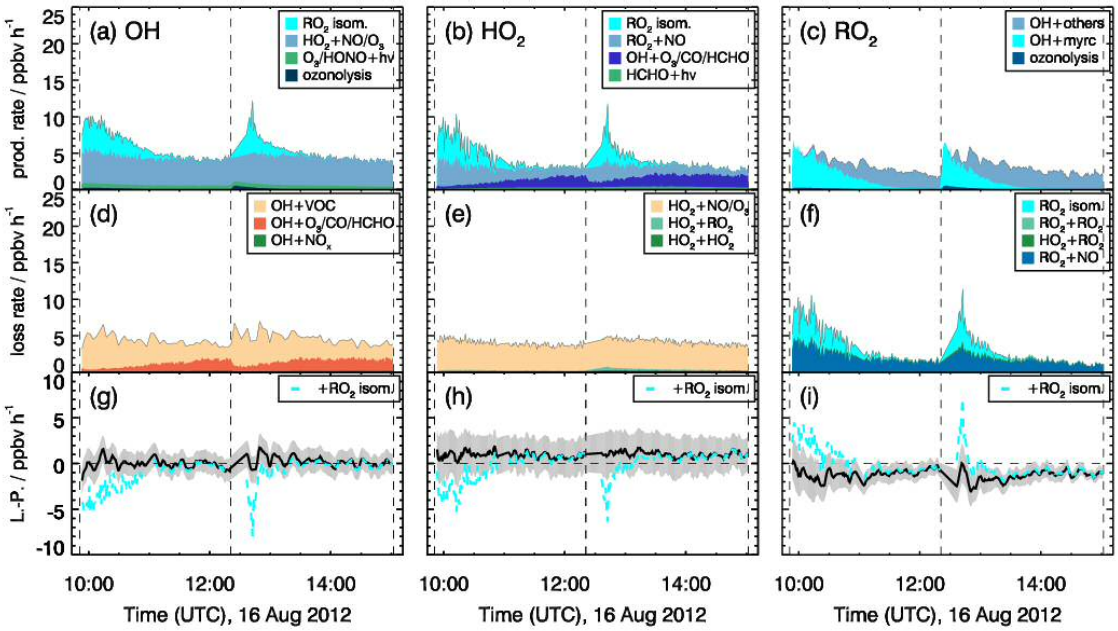

Figure 7. Rates of radical conversion reactions and imbalances between production and destruction rates ($L - P$) for the experiment with medium NO mixing ratios on 16 August 2012. Grey areas in the lower panels give the uncertainty of $L - P$. In the lowest right panel, the black and cyan lines denote RO_2 budget without and with considering MyO_2 isomerization reaction at a rate of $0.014\,s^{-1}$.

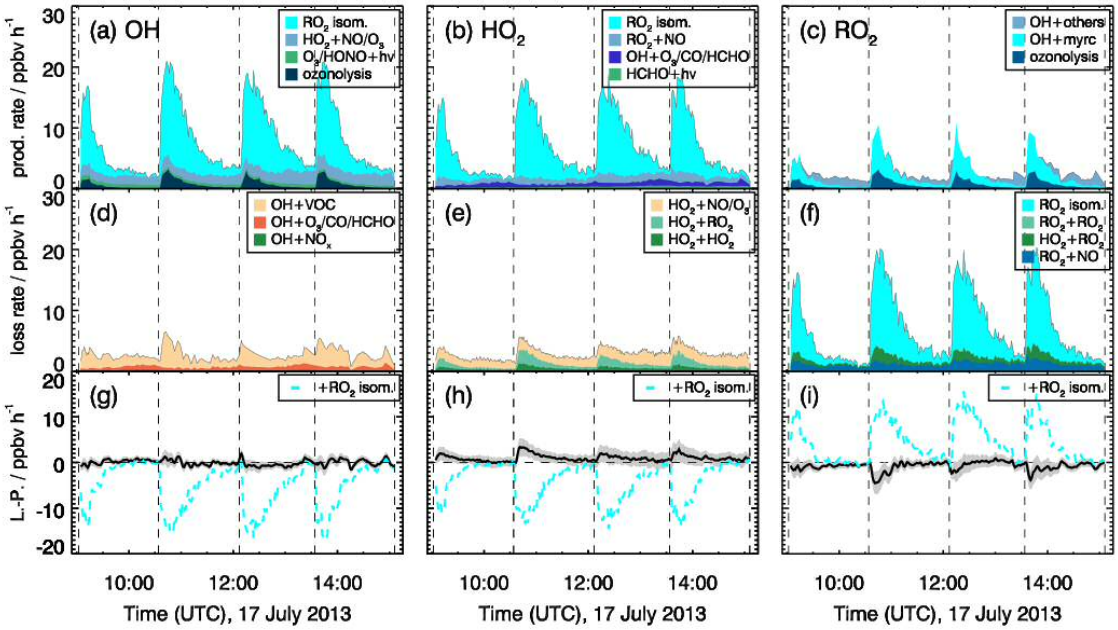

Figure 8. Same as Fig. S7, but for the experiment with myrcene at low NO conditions on 17 July 2013.